LEGIBILITY NOTICE

A major purpose of the Technical Information Center is to provide the broadest dissemination possible of information contained in DOE's Research and Development Reports to business, industry, the academic community, and federal, state and local governments.

Although a small portion of this report is not reproducible, it is being made available to expedite the availability of information on the research discussed herein.

1

ORNL-6561

OAK RIDGE NATIONAL LABORATORY

MARTIN MARIETTA

Neutron Capture of ^{122}Te, ^{123}Te, ^{124}Te, ^{125}Te, and ^{126}Te

R. L. Macklin
R. R. Winters

OPERATED BY
MARTIN MARIETTA ENERGY SYSTEMS, INC.
FOR THE UNITED STATES
DEPARTMENT OF ENERGY

ORNL--6561

DE89 015682

Engineering Physics and Mathematics Division

NEUTRON CAPTURE OF ^{122}Te, ^{123}Te, ^{124}Te, ^{125}Te, AND ^{126}Te

R. L. Macklin and R. R. Winters*

*Department of Physics, Denison University, Granville, OH 43203

DATE PUBLISHED — JULY 1989

Prepared for the
Office of Energy Research
Nuclear Physics

Prepared by the
OAK RIDGE NATIONAL LABORATORY
Oak Ridge, Tennessee 37831
operated by
MARTIN MARIETTA ENERGY SYSTEMS, INC.
for the
U.S. DEPARTMENT OF ENERGY
under contract DE-AC05-84OR21400

CONTENTS

ACKNOWLEDGMENTS

The ORELA operators and engineers faithfully provided the pulsed neutrons used for all the measurements. S. R. Damewood prepared the text and tables for publication. One of the authors (R.R.W.) particularly thanks Stanley Whetstone, U.S. Department of Energy, for his support and interest. This work was sponsored by the U.S. Department of Energy under contracts DE-FG02-87ER40326 with Denison University and DE-AC05-84OR21400 with Martin Marietta Energy Systems Inc.

ABSTRACT

Isotopically enriched samples of the tellurium isotopes from mass 122 to mass 126 were used to measure neutron capture in the energy range 2.6 keV to 600 keV at the Oak Ridge Electron Linear Accelerator pulsed neutron source. Starting at 2.6 keV, over 200 Breit-Wigner resonances for each isotope were used to describe the capture data. Least-squares adjustment gave parameters and their uncertainties for a total of 1659 resonances. Capture cross sections averaged over Maxwellian neutron distributions with temperatures ranging from $kT = 5$ keV to $kT = 100$ keV were derived for comparison with stellar nucleosynthesis calculations. For the three isotopes shielded from the astrophysical r-process, ^{122}Te, ^{123}Te and ^{124}Te at $kT = 30$ keV the respective values were (280 ± 10) mb, (819 ± 30) mb and (154 ± 6) mb. The corresponding products of cross section and solar system abundance are nearly equal in close agreement with s-process nucleosynthesis calculations.

1. INTRODUCTION

The stable isotopes heavier than iron are thought to be byproducts of nuclear fusion in stars. The stars generate energy by combining the lightest and most abundant element, hydrogen, into more and more tightly bound nuclei up to nickel and iron at mass 56. Beyond that point the heavier nuclei are less tightly bound, breaking up spontaneously beyond lead and bismuth at mass 208 and 209. Two of the light element reactions, ^{13}C (α, n) and ^{22}Ne(α, n) have been identified as likely sources of neutrons which then by capture on successively heavier nuclei can build up the elements beyond iron. Detailed theories of stellar nucleosynthesis continue to be developed, following their first monumental synthesis by Burbidge et al. (1957).

Although nucleosynthesis reactions take place deep in the interiors of stars, their products are visible at the surface. However, the most detailed information on abundances comes from the debris of exploded stars that has been incorporated in our solar system and the earth. The elemental abundances in the meteorites and the earth's crust appear to have been modified by thermal and chemical processes but the relative abundance of the heavy stable isotopes therein appears remarkably uniform. Slight changes in isotopic abundance evaluations over the years reflect the refinement of measurements and in a few instances an improved evaluation of the slow radioactive decays that have occurred over the 4.6-billion-year life of the solar system. A recent review of the meteoritic and solar system abundances has been prepared by Anders and Grevesse (1989).

When neutrons are accumulated slowly, nucleosynthesis proceeds by the s-process of Burbidge et al. (1957), most radioactive isotopes have time for beta decay to the next higher chemical element so that the process follows the 'valley of stability' to the heavier elements. For this process the amount of an isotope remaining is inversely proportional to its probability of absorbing another neutron. This probability can be found by measuring the capture cross section in the laboratory as a function of neutron energy and averaging over the Maxwellian spread of neutron energies at a temperature sufficient to produce neutrons from the light element reactions mentioned above. Some stellar processes such as the r-process of Burbidge et al. (1957) proceed much more rapidly and can produce neutron rich radioactive isotopes which subsequently decay to the heaviest stable isotope of the same mass by beta emission. Most of the stable isotopes heavier than iron that we find in the earth's crust were produced by one or both of these processes in stars which had long since passed through their main sequence and red giant stages to become faint white dwarfs or supernova debris. In many cases an element will have a stable isotope with the same atomic mass as a stable isotope of an element with a slightly lower atomic number. Thus it is shielded from the r-process and is known as an s-only isotope. For a few elements there is a pair of such isotopes and in one case, tellurium, there are three. Because of the absence of isotopic fractionation in solar system material these multiplets have provided especially stringent tests of s-process calculations (Macklin and Gibbons, 1967a,b). Summaries of neutron capture cross sections for s-process studies have appeared frequently, most recently by Bao and Käppeler (1987). Neutron capture by isotopes of tellurium, including the three s-only ones has been measured by Bergman and Romanov (1974) at energies up to 40 keV. Bao and Käppeler (1987) suggest that for reliable calculations of

Maxwellian averaged cross sections near $kT = 30$ keV, a temperature typical of the inner regions of stars, differential neutron capture data are needed up to 250 keV.

The present measurements cover a neutron energy range 2.6 keV to 600 keV. Capture peaks were fitted to Breit-Wigner single level parameters above 2.6 keV and Maxwellian average capture cross sections were derived from $kT = 5$ keV to $kT = 100$ keV. These data provide additional and more accurate values which can serve as tests for models of nucleosynthesis in stars.

2. EXPERIMENTAL PROCEDURE

Neutron capture was measured at the ORELA pulsed neutron time-of-flight facility. The neutrons were produced from tantalum by bremstrahlung from brief bursts of ~140 MeV electrons and reduced in energy by elastic scattering in a water moderator. Samples were exposed to the neutrons 40 meters from the moderator where the beam size had been restricted by copper collimators to a rectangle about 28 mm by 56 mm. Neutrons below 7 eV were strongly absorbed by a filter containing 4.8 mg/mm^2 of ^{10}B early in the flight path. Neutron capture gamma-rays were detected by a pair of fluorocarbon scintillators close to the sample but outside the neutron beam. The neutron flux was monitored by a 1/2-mm-thick piece of ^{6}Li glass scintillator as well as the ORELA flux monitor. An illustration of the apparatus was included in a previous report on tungsten (Macklin, Drake, and Arthur, 1983).

Pulse-height weighting was used to measure the total prompt gamma-ray energy release. Dividing this energy release by the neutron binding plus kinetic energy per compound nucleus gave the number of neutrons captured. Dividing by the number of isotope atoms in the sample and the incident neutron flux led then to an effective neutron capture cross section. A more extensive description of the use of the apparatus and procedures can be found in a recent report on neutron capture by rubidium isotopes (Beer and Macklin, 1989).

Each sample was mounted between the two detectors, facing the neutron source and at an effective flight path of 40121 mm. Measurements on each isotope in turn were accomplished in 171 hours of ORELA beam time and then the measurements were repeated, using another 166 hours of beam time as a check of reproducibility. The accelerator operated at 800 pulses per second with a full width at half-maximum of six nanoseconds and a beam power of 10–12 kilowatts. Cross-section calibration was done by the saturated 4.9-eV gold resonance method (Macklin, Halperin and Winters, 1979) before each set of measurements. The saturated resonance intercalibration technique has been used with several suitable isotopes in the past, showing ±1% agreement for holmium, gold, and ^{238}U (Macklin, 1976b). Yamamuro et al. (1976) have found similar agreement between ^{197}Au and ^{109}Ag.

The extension of the neutron flux shape from the 4.9 eV intercalibration energy to 1 MeV (Macklin, Ingle and Halperin, 1979) involves the ^{6}Li(n, α) cross section up to 70 keV and the ^{235}U fission cross section above 3 keV. Uncertainty components involved in using the ENDF/B-V files and an experimental intercomparison of the lithium glass scintillator with a ^{235}U fission chamber have been discussed and tabulated previously (Macklin, 1984).

3. SAMPLES

Enriched samples of five stable isotopes ranging in atomic mass from 122 to 126 were obtained as pressed metal powder about 26.1 mm × 26.2 mm in area and 2 mm in thickness. These were made from stocks of amorphous metal powder. Difficulties were reported in pressing the samples of enriched ^{123}Te and ^{124}Te and samples from other batches were substituted before satisfactory pressed samples were delivered. All samples were close to 6 g when pressed. We suspect that exposure to air led to appreciable formation of the dioxide TeO_2 since when the sample containers were opened and neutron capture measurements started, all the samples had gained weight, particularly the ^{122}Te and ^{124}Te which had increased 16% and 12% respectively. As the measurements were made in vacuum at room temperature, adsorbed moisture could not have been significant. Subsequent vacuum bakeout of the ^{122}Te sample at 75°C and then again at 125°C was not effective in reducing the weight. The samples that gained the most weight did not crumble or appear any different than the others except for a greater thickness, comparable to the weight gain. Searches for signs of increased neutron scattering at the 440-keV oxygen resonance as evidenced in the neutron capture yields were inconclusive.

Chemical reanalysis of the tellurium content of each sample confirmed the original masses. Sample recovery averaged 98% for the four heavier isotope samples but more than a gram of the ^{122}Te sample was lost in recovery due to a 'bad reagent'. Clearly, elemental tellurium samples are not stable against oxidation in air. Details of the sample parameters and analyses are summarized in Table 1.

Table 1. Enriched Tellurium Isotope Samples

Sample	1	2	3	4	5
Height (mm)	26.1	26.2	26.2	26.2	26.1
Width (mm)	26.1	26.1	26.1	26.1	26.1
Thickness (mm)	0.20	0.17	0.20	0.18	0.17
Weight[a] (g)	5.969	5.983	5.990	6.052	5.983
Impurities[a,b] (wt %)	0.05	0.11	0.01		
^{122}Te/Te[c]	0.9712	0.0156	0.0012	0.0003	<0.0002
^{123}Te/Te	0.0015	0.7667	0.0010	0.0006	<0.0002
^{124}Te/Te	0.0023	0.0696	0.9300	0.0028	0.0005
^{125}Te/Te	0.0028	0.0336	0.0105	0.9567	0.0020
^{126}Te/Te	0.0070	0.0435	0.0410	0.0271	0.9869
^{128}Te/Te	0.0106	0.0396	0.0100	0.0076	0.0081
^{130}Te/Te	0.0046	0.0315	0.0063	0.0049	0.0024

[a]Exclusive of oxide formation – see text.

[b]Limits of detectability for individual elements ranged from 0.002 to 0.1. Elements detected include Si, Mg, Ag, Cu, and Sn.

[c]^{120}Te/Te was <0.0005.

4. DATA PROCESSING

Corrections applied to the data include electronic dead-time loss and amplifier gain standardization, average scattered neutron backgrounds, gamma-energy loss in the sample, average resonance self-protection and scattering before capture in the sample. Uncertainty estimates are discussed in Section 7.

Capture yields from each of the five enriched samples were combined linearly to remove the contributions of minor isotopes in each, leaving the yield of the most highly enriched isotope contaminated only by the traces of ^{128}Te and ^{130}Te present. Only the largest capture peaks from these two heavier isotopes could be discerned in our data for ^{122}Te, ^{123}Te, ^{124}Te and ^{126}Te. The ^{128}Te peak at 3268 eV was sufficiently isolated in the ^{122}Te data for least squares fitting of its parameters as seen in Fig. 1. The capture kernel found, $g\Gamma_\gamma\Gamma_n/\Gamma = (80 \pm 20)$ meV, is not significantly larger than the (62.0 ± 12.4) meV reported using enriched ^{128}Te (Browne and Berman, 1973).

ORNL-DWG 89-11737

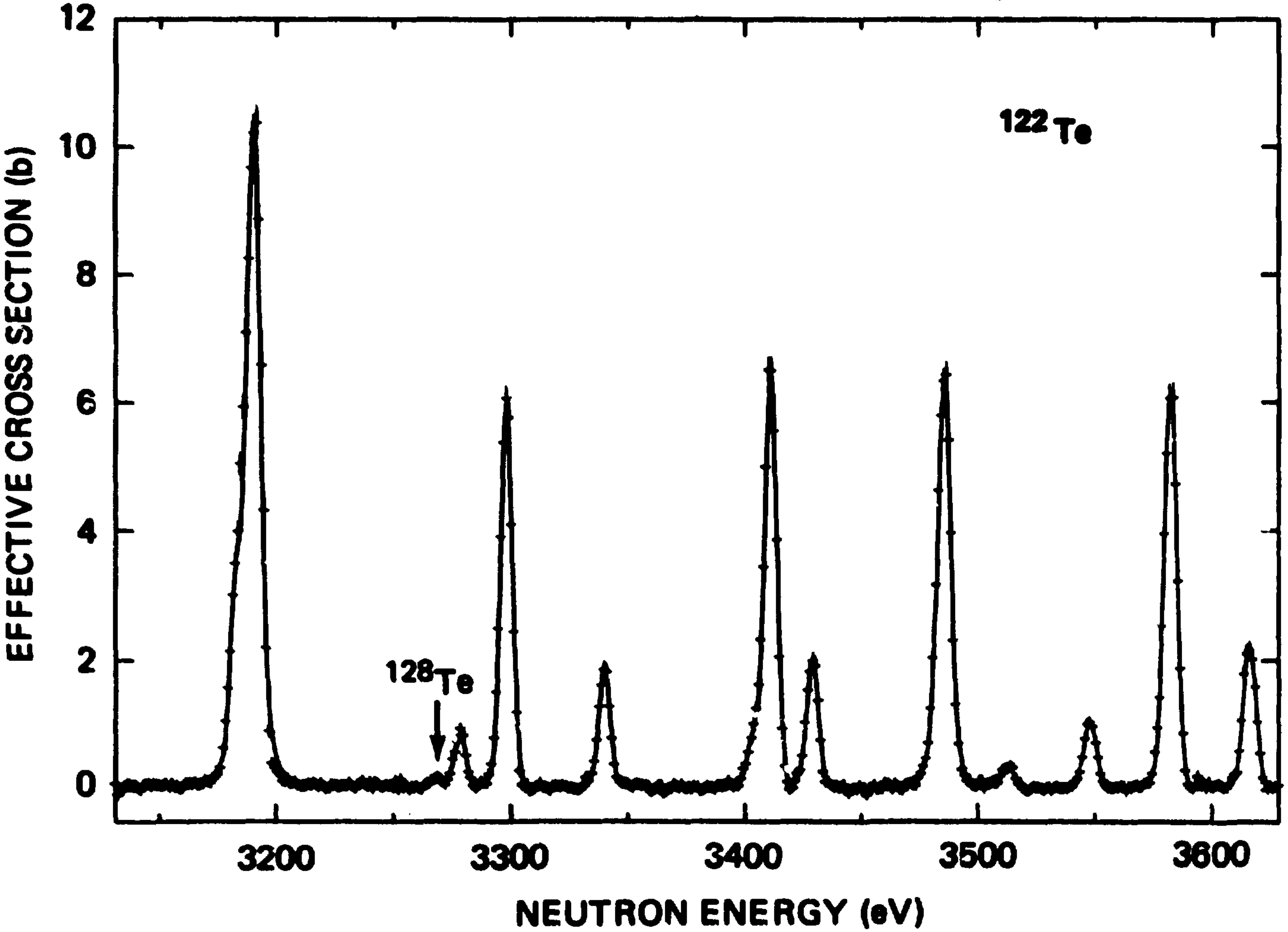

Fig. 1. The ^{122}Te neutron capture data near 3 keV. The symbols represent the data points and their statistical standard deviations. The solid curve corresponds to the fitted parameters given in the tables except for the small ^{128}Te impurity peak at 3268 eV discussed in the text.

5. INDIVIDUAL RESONANCE PARAMETERIZATION

The resonance analysis was carried out by fitting peaks in the capture yield data with the least-squares fitting code LSFIT (Macklin, 1976a). The code provided Breit-Wigner single-level parameters and statistical standard deviations for those parameters that were adjusted. The symmetric capture cross section for each resonance was Doppler-broadened using the real part of the complex error function. Attenuation by successive layers of a sample was approximated by the same symmetric shape for the resonance total cross section plus an energy independent potential scattering cross section. Parameters found from fitting the capture data are listed in Tables 2–7.

For ^{122}Te, in addition to the resonance capture kernels $g\Gamma_\gamma\Gamma_n/\Gamma$, there were 30 resonances below 12 keV broad enough to fit the total width and, assigning these $l = 0$, $J = 1/2$, to find neutron and radiation widths separately. The average radiation width found was $\Gamma_\gamma = (73.3 \pm 4.3)$ meV with a standard deviation per resonance of 23.3 meV, corresponding to a chi-square distribution with 20 degrees of freedom. From 12 keV to 16.5 keV 20 resonances showed much stronger capture and were assigned $l = 1$, $J = 3/2$. Two of these were considered probable doublets and excluded. The other 18 gave an average radiation width $\Gamma_\gamma = (71.8 \pm 4.7)$ meV, not significantly different from the $l = 0$ average found above. With a change of assignment to $J = 1/2$, of course the average radiation width for these 18 resonances would have been twice as large. The standard deviation for the $J = 3/2$ distribution was 19.9 meV corresponding to a chi square with 26 degrees of freedom, again very similar to the $l = 0$ distribution. Above 16.5-keV neutron energy the resonance peaks were increasingly crowded together and the attempt to fit individual peaks was terminated at 20 keV. Examples of the data and fitting are shown in Figs. 1 and 2.

For ^{123}Te there were no previous resonance parameters in our energy range. Ten peaks below 6 keV were broad enough to fit total widths assuming $l = 0$, $J = 1$. These gave an average radiation width $\Gamma_\gamma = (116 \pm 8)$ meV with a standard deviation of 26 meV, corresponding to a chi square distribution with 40 degrees of freedom. One resonance at 3.855 keV was fitted assuming $J = 0$, finding a radiation width of 122 meV rather than the 41 meV corresponding to a $J = 1$ choice. The resonance analysis was extended up to 7.65 keV.

For ^{124}Te fifteen resonances up to 10 keV were fitted as singlets assuming $l = 0$, $J = 1/2$. These included four where the capture data could not distinguish a total width but the earlier transmission data evaluation (Mughabghab, 1984) gave neutron widths greater than 500 meV. The average radiation width found was $\Gamma_\gamma = (63.5 \pm 5.3)$ meV with a standard deviation of 20.6 meV corresponding to a chi square distribution with 19 degrees of freedom. The resonance analysis was continued up to 41 keV.

Table 2. ^{122}Te Resonance Capture Parameters

E_n (keV)	$g\Gamma_n\Gamma_\gamma/\Gamma$ (meV)	E_n (keV)	$g\Gamma_n\Gamma_\gamma/\Gamma$ (meV)	E_n (keV)	$g\Gamma_n\Gamma_\gamma/\Gamma$ (meV)
2.708[a]	6.6 ± 0.2[b]	4.513	4.0 ± 0.3	6.388	1.5 ± 0.5
2.737	25.2 ± 0.4	4.530	30.2 ± 0.7	6.433	45.7 ± 1.4
2.762	22.1 ± 0.3	4.545	7.6 ± 0.4	6.497	30.6 ± 1.9
2.793	4.8 ± 0.2	4.617	44.3 ± 0.8	6.503	27.1 ± 2.0
2.868	64.0 ± 1.1	4.657	19.2 ± 0.6	6.536	61.2 ± 2.5
2.920	17.4 ± 0.4	4.683	3.8 ± 0.3	6.571	3.2 ± 0.6
2.927	11.8 ± 0.4	4.767	62.4 ± 1.5	6.636	21.5 ± 1.0
2.942	40.5 ± 0.5	4.808	16.1 ± 0.6	6.679	45.7 ± 1.4
2.968	53.2 ± 1.0	4.824	46.9 ± 1.0	6.690	11.4 ± 1.3
2.987	4.1 ± 0.2	4.854	58.0 ± 1.7	6.711	56.0 ± 1.5
3.009	2.8 ± 0.2	4.941	43.7 ± 0.8	6.749	15.6 ± 0.9
3.086	2.6 ± 0.2	5.011	66.3 ± 1.7	6.786	43.0 ± 1.2
3.095	18.2 ± 0.4	5.026	31.6 ± 0.8	6.817	45.7 ± 1.1
3.114	28.5 ± 0.4	5.056	13.2 ± 0.6	6.838	1.4 ± 0.6
3.122	2.4 ± 0.2	5.067	12.0 ± 0.6	6.906	47.8 ± 1.3
3.183	11.7 ± 0.5	5.097	47.5 ± 1.0	6.923	18.2 ± 0.8
3.190	102.6 ± 1.6	5.164	20.9 ± 0.7	6.979	32.9 ± 1.0
3.278	4.3 ± 0.2	5.176	39.1 ± 0.8	7.016	55.2 ± 1.7
3.298	31.8 ± 0.5	5.201	4.0 ± 0.4	7.028	46.1 ± 2.6
3.340	9.8 ± 0.3	5.261	13.3 ± 0.7	7.059	110.0 ± 6.7
3.404	4.0 ± 0.3	5.299	43.1 ± 1.0	7.134	37.1 ± 1.1
3.411	36.2 ± 0.6	5.317	37.0 ± 0.9	7.166	72.9 ± 1.6
3.429	21.1 ± 0.4	5.335	90.2 ± 2.1	7.185	51.9 ± 1.5
3.486	54.8 ± 1.4	5.402	18.6 ± 0.7	7.248	16.6 ± 0.8
3.513	2.0 ± 0.2	5.443	33.2 ± 0.9	7.293	55.7 ± 1.2
3.548	6.2 ± 0.3	5.482	60.4 ± 1.8	7.309	12.2 ± 0.9
3.582	37.9 ± 0.7	5.539	21.6 ± 0.8	7.352	51.6 ± 1.2
3.616	13.6 ± 0.4	5.584	11.5 ± 0.6	7.364	18.3 ± 1.2
3.650	2.3 ± 0.2	5.631	4.9 ± 0.5	7.426	9.3 ± 0.6
3.672	41.0 ± 0.5	5.685	3.4 ± 0.8	7.481	7.1 ± 0.6
3.705	55.9 ± 1.2	5.693	37.6 ± 1.1	7.566	16.1 ± 0.7
3.736	40.2 ± 0.6	5.708	24.8 ± 1.0	7.633	81.5 ± 1.6
3.747	1.6 ± 0.2	5.750	3.2 ± 0.5	7.650	44.0 ± 1.3
3.786	3.5 ± 0.2	5.791	84.0 ± 2.6	7.663	39.5 ± 1.3
3.852	51.4 ± 0.6	5.881	33.9 ± 1.1	7.691	41.9 ± 1.2
3.944	2.5 ± 0.2	5.940	30.9 ± 1.0	7.766	35.6 ± 1.1
3.993	60.5 ± 1.5	5.956	22.5 ± 0.9	7.831	46.8 ± 1.3
4.053	3.8 ± 0.2	6.029	84.0 ± 1.6	7.850	18.4 ± 1.3
4.067	6.0 ± 0.3	6.109	3.1 ± 0.6	7.873	54.6 ± 3.5
4.084	0.7 ± 0.2	6.131	50.1 ± 2.0	7.921	42.0 ± 1.2
4.127	13.4 ± 0.4	6.158	33.0 ± 1.2	8.035	4.0 ± 0.9
4.175	33.9 ± 0.6	6.175	60.5 ± 1.6	8.051	25.8 ± 1.3
4.194	3.9 ± 0.3	6.246	43.3 ± 2.2	8.067	46.9 ± 1.5
4.214	65.6 ± 2.6	6.318	3.5 ± 0.6	8.083	7.0 ± 1.5
4.280	90.7 ± 2.4	6.339	47.9 ± 1.3	8.113	9.6 ± 0.8
4.343	5.2 ± 0.4	6.352	51.3 ± 1.4	8.180	51.7 ± 2.4
4.448	43.0 ± 1.3	6.367	3.7 ± 0.7	8.205	32.7 ± 1.2

Table 2. Continued

E_n (keV)	$g\Gamma_n\Gamma_\gamma/\Gamma$ (meV)	E_n (keV)	$g\Gamma_n\Gamma_\gamma/\Gamma$ (meV)	E_n (keV)	$g\Gamma_n\Gamma_\gamma/\Gamma$ (meV)
8.227	1.6 ± 0.6	9.995	50.6 ± 1.5	11.98	51.1 ± 1.9
8.277	56.8 ± 2.4	10.02	4.6 ± 0.8	12.04	15.5 ± 1.4
8.338	70.3 ± 2.9	10.08	46.3 ± 1.4	12.09	153.2 ± 3.1
8.349	29.9 ± 1.8	10.15	8.4 ± 0.9	12.14	14.4 ± 1.3
8.381	39.8 ± 1.2	10.18	51.8 ± 1.7	12.18	52.1 ± 1.8
8.437	51.3 ± 1.6	10.22	38.3 ± 1.3	12.22	53.3 ± 2.0
8.452	27.8 ± 1.8	10.24	16.5 ± 1.0	12.27	58.2 ± 2.3
8.464	42.0 ± 1.8	10.28	7.0 ± 1.4	12.35	145.4 ± 3.7
8.507	4.6 ± 0.7	10.29	44.7 ± 1.4	12.41	55.5 ± 2.6
8.549	32.2 ± 1.2	10.33	24.3 ± 1.0	12.43	15.1 ± 2.7
8.577	55.5 ± 1.3	10.38	5.2 ± 0.7	12.45	49.1 ± 2.5
8.609	6.5 ± 0.7	10.42	95.7 ± 2.0	12.49	6.4 ± 2.1
8.650	3.7 ± 0.6	10.45	105.4 ± 2.7	12.51	41.3 ± 2.2
8.703	92.8 ± 1.7	10.47	84.6 ± 1.5	12.56	13.4 ± 1.5
8.731	43.3 ± 1.3	10.60	114.5 ± 3.7	12.65	123.4 ± 4.0
8.819	7.2 ± 0.8	10.63	44.5 ± 1.3	12.68	162.0 ± 4.2
8.843	47.8 ± 1.3	10.67	9.9 ± 0.9	12.72	48.2 ± 2.1
8.878	20.9 ± 1.5	10.70	6.9 ± 0.8	12.75	20.8 ± 1.8
8.892	37.2 ± 1.4	10.74	12.5 ± 1.4	12.80	79.0 ± 2.8
8.967	45.0 ± 1.3	10.76	44.7 ± 1.4	12.85	170.4 ± 4.3
8.993	34.5 ± 1.1	10.82	104.9 ± 2.7	12.89	54.7 ± 2.5
9.038	27.0 ± 1.1	10.88	69.9 ± 2.4	12.92	28.1 ± 2.7
9.073	59.2 ± 1.7	10.90	21.5 ± 1.8	12.96	44.6 ± 4.1
9.093	40.4 ± 1.2	10.99	109.6 ± 4.1	12.98	99.3 ± 4.6
9.115	13.9 ± 1.0	11.02	40.9 ± 2.0	13.05	177.1 ± 8.7
9.154	64.7 ± 1.5	11.07	10.2 ± 1.1	13.18	50.0 ± 2.6
9.235	56.4 ± 2.7	11.12	37.8 ± 1.7	13.24	40.7 ± 2.8
9.293	26.0 ± 1.1	11.15	23.9 ± 1.6	13.28	51.1 ± 2.7
9.339	11.2 ± 0.8	11.20	55.7 ± 2.0	13.34	56.6 ± 3.0
9.372	36.6 ± 1.2	11.28	18.9 ± 2.0	13.49	122.4 ± 4.7
9.422	39.2 ± 2.2	11.30	45.1 ± 2.0	13.52	35.8 ± 2.6
9.435	66.9 ± 2.1	11.33	20.0 ± 1.7	13.59	79.4 ± 4.3
9.469	94.3 ± 2.1	11.36	36.3 ± 2.0	13.62	25.4 ± 3.6
9.486	49.5 ± 1.8	11.38	20.5 ± 1.8	13.68	18.0 ± 2.3
9.530	50.5 ± 1.5	11.42	81.4 ± 2.5	13.78	55.6 ± 3.0
9.565	51.7 ± 1.4	11.45	87.1 ± 2.7	13.81	52.1 ± 3.0
9.639	65.0 ± 1.8	11.53	94.6 ± 2.7	13.86	54.0 ± 3.2
9.654	17.3 ± 1.6	11.58	55.2 ± 1.8	13.90	141.3 ± 4.9
9.668	11.2 ± 1.3	11.63	13.2 ± 1.3	13.97	50.4 ± 2.5
9.700	16.9 ± 1.1	11.66	59.9 ± 2.1	14.01	91.8 ± 4.6
9.746	3.8 ± 0.8	11.69	23.0 ± 1.9	14.03	92.6 ± 3.7
9.797	69.2 ± 2.7	11.74	83.4 ± 3.8	14.18	54.3 ± 3.1
9.821	10.9 ± 1.4	11.79	36.4 ± 2.9	14.20	50.9 ± 3.4
9.837	58.0 ± 1.7	11.81	20.6 ± 2.3	14.23	22.6 ± 3.0
9.894	28.4 ± 1.4	11.85	49.7 ± 1.9	14.26	95.1 ± 4.2
9.916	35.9 ± 1.4	11.90	7.9 ± 1.8	14.28	20.5 ± 3.2
9.967	44.2 ± 1.6	11.92	47.1 ± 2.0	14.34	154.6 ± 6.4

Table 2. Continued

E_n (keV)	$g\Gamma_n\Gamma_\gamma/\Gamma$ (meV)	E_n (keV)	$g\Gamma_n\Gamma_\gamma/\Gamma$ (meV)	E_n (keV)	$g\Gamma_n\Gamma_\gamma/\Gamma$ (meV)
14.39	54.8 ± 3.0	16.17	116.9 ± 4.0	18.03	101.5 ± 6.2
14.49	65.6 ± 2.9	16.21	39.5 ± 2.9	18.08	116.4 ± 6.6
14.54	100.2 ± 3.5	16.29	111.1 ± 4.3	18.17	119.5 ± 6.9
14.57	31.6 ± 2.5	16.32	42.1 ± 3.5	18.27	183.4 ± 5.7
14.63	291.5 ± 9.2	16.37	28.6 ± 2.8	18.35	174.5 ± 9.4
14.70	174.0 ± 6.7	16.43	111.1 ± 7.7	18.39	105.8 ± 6.2
14.77	59.8 ± 2.9	16.56	194.0 ± 8.0	18.47	4.7 ± 2.3
14.81	7.7 ± 1.9	16.63	96.2 ± 4.3	18.52	158.6 ± 11.0
14.85	54.5 ± 2.9	16.74	175.2 ± 8.4	18.54	111.5 ± 9.8
14.88	68.1 ± 4.2	16.79	57.9 ± 3.2	18.64	28.6 ± 2.6
14.90	92.4 ± 3.5	16.86	79.9 ± 4.0	18.71	221.1 ± 7.9
14.93	71.4 ± 3.3	16.90	157.4 ± 5.7	18.79	69.9 ± 4.3
14.98	230.8 ± 7.6	16.96	63.8 ± 5.2	18.84	185.5 ± 7.5
15.02	53.9 ± 2.7	16.99	93.7 ± 5.0	18.91	135.1 ± 7.8
15.10	122.2 ± 6.1	17.02	66.2 ± 4.1	18.98	168.3 ± 5.5
15.17	89.7 ± 5.6	17.07	91.2 ± 4.1	19.05	157.4 ± 7.2
15.23	78.5 ± 2.9	17.12	61.4 ± 3.6	19.09	89.8 ± 5.4
15.34	110.2 ± 3.3	17.18	142.8 ± 8.4	19.19	141.8 ± 8.5
15.41	54.3 ± 2.5	17.24	48.4 ± 4.3	19.26	65.5 ± 5.4
15.55	162.3 ± 6.3	17.28	25.2 ± 4.3	19.30	91.8 ± 5.6
15.63	84.9 ± 3.2	17.33	65.1 ± 4.5	19.34	71.1 ± 5.3
15.67	54.6 ± 4.1	17.41	100.3 ± 6.8	19.38	52.5 ± 6.0
15.69	57.0 ± 3.5	17.46	139.0 ± 10.3	19.49	65.4 ± 17.0
15.72	42.7 ± 3.1	17.51	10.2 ± 3.9	19.51	215.8 ± 21.9
15.78	109.5 ± 3.5	17.61	113.0 ± 8.5	19.59	100.5 ± 5.7
15.84	104.2 ± 3.4	17.64	51.4 ± 7.3	19.64	91.4 ± 8.2
15.88	53.1 ± 4.4	17.66	33.0 ± 6.4	19.66	99.0 ± 7.5
15.90	30.7 ± 3.5	17.74	83.8 ± 5.3	19.72	58.5 ± 11.5
15.96	39.1 ± 2.7	17.79	169.3 ± 7.4	19.80	51.9 ± 4.2
16.02	18.3 ± 2.1	17.84	51.1 ± 7.0	19.88	236.4 ± 7.8
16.10	233.5 ± 8.9	17.89	350.9 ± 12.4	19.93	41.9 ± 5.2
16.14	54.2 ± 3.3	17.96	80.8 ± 7.5	20.00	330.9 ± 10.7

[a]Resonances below 2.6 keV were not included in the present work.

[b]Statistical standard deviations determined by the least squares data fitting program. Systematic uncertainties are estimated at 3.6%.

Table 3. ^{123}Te Resonance Capture Parameters

E_n (keV)	$g\Gamma_n\Gamma_\gamma/\Gamma$ (meV)	E_n (keV)	$g\Gamma_n\Gamma_\gamma/\Gamma$ (meV)	E_n (keV)	$g\Gamma_n\Gamma_\gamma/\Gamma$ (meV)
2.672[a]	46.8 ± 2.2[b]	3.297	9.4 ± 0.4	3.915	43.7 ± 1.1
2.708	4.8 ± 0.4	3.322	2.8 ± 0.3	3.928	11.9 ± 0.5
2.713	11.6 ± 0.4	3.333	14.5 ± 0.5	3.937	13.8 ± 0.6
2.719	4.1 ± 0.3	3.353	8.6 ± 0.5	3.947	15.9 ± 1.2
2.731	9.4 ± 0.6	3.361	21.5 ± 0.6	3.951	40.9 ± 1.2
2.734	10.4 ± 0.6	3.383	14.3 ± 0.6	3.966	2.5 ± 0.3
2.738	10.4 ± 0.5	3.391	43.9 ± 0.8	3.980	1.3 ± 0.3
2.747	4.7 ± 0.4	3.412	3.8 ± 0.6	3.998	23.5 ± 0.7
2.751	15.1 ± 0.5	3.417	52.8 ± 0.9	4.005	3.4 ± 0.6
2.776	5.8 ± 0.2	3.426	4.7 ± 0.4	4.022	12.0 ± 0.5
2.799	6.0 ± 0.3	3.434	7.2 ± 0.7	4.033	9.0 ± 0.9
2.808	6.9 ± 0.5	3.440	53.4 ± 0.9	4.038	38.5 ± 1.1
2.813	52.1 ± 0.3	3.453	61.1 ± 0.9	4.050	8.0 ± 0.5
2.822	4.9 ± 0.3	3.470	37.5 ± 0.7	4.057	4.7 ± 0.8
2.830	1.4 ± 0.2	3.502	88.1 ± 2.0	4.063	28.8 ± 0.8
2.846	1.8 ± 0.2	3.512	3.9 ± 0.5	4.084	1.9 ± 0.5
2.865	5.6 ± 0.4	3.527	7.5 ± 1.1	4.091	7.3 ± 0.7
2.871	41.9 ± 1.1	3.531	57.9 ± 1.4	4.099	26.5 ± 0.7
2.878	9.2 ± 0.3	3.548	44.0 ± 0.8	4.116	3.4 ± 0.5
2.890	1.6 ± 0.2	3.564	3.9 ± 0.8	4.124	29.4 ± 0.7
2.917	7.6 ± 0.3	3.569	47.6 ± 1.0	4.140	49.7 ± 0.9
2.924	14.6 ± 0.4	3.586	2.1 ± 0.4	4.170	6.4 ± 0.4
2.935	25.6 ± 0.4	3.596	57.2 ± 0.9	4.208	10.8 ± 0.6
2.948	73.6 ± 2.4	3.618	1.7 ± 0.3	4.217	25.4 ± 0.7
2.958	10.0 ± 0.5	3.625	1.9 ± 0.4	4.232	12.5 ± 0.6
2.964	58.1 ± 0.3	3.631	6.0 ± 0.7	4.239	3.8 ± 0.6
2.971	1.9 ± 0.2	3.637	38.0 ± 0.9	4.255	8.3 ± 0.6
2.978	12.4 ± 0.3	3.644	10.6 ± 0.8	4.265	52.1 ± 0.9
2.990	11.9 ± 0.6	3.659	17.7 ± 0.6	4.274	4.2 ± 0.5
2.993	5.5 ± 0.6	3.676	3.6 ± 0.5	4.280	2.4 ± 0.4
3.026	8.6 ± 0.3	3.682	4.3 ± 0.6	4.298	3.7 ± 0.5
3.038	2.8 ± 0.2	3.692	95.8 ± 1.9	4.305	28.2 ± 0.7
3.057	83.5 ± 3.0	3.710	58.2 ± 1.0	4.327	4.3 ± 0.9
3.071	41.5 ± 1.0	3.726	27.8 ± 1.0	4.332	13.8 ± 0.9
3.087	52.8 ± 1.1	3.734	68.4 ± 1.2	4.339	16.1 ± 0.8
3.100	3.2 ± 0.7	3.742	9.5 ± 0.7	4.348	71.3 ± 1.1
3.106	6.4 ± 0.6	3.766	8.4 ± 0.5	4.356	3.8 ± 0.7
3.114	13.8 ± 0.7	3.790	1.7 ± 0.3	4.374	67.6 ± 1.0
3.123	24.1 ± 0.8	3.805	53.4 ± 0.9	4.398	65.8 ± 1.5
3.154	51.8 ± 1.1	3.821	5.1 ± 0.4	4.410	10.9 ± 0.8
3.164	8.8 ± 0.5	3.835	30.1 ± 1.2	4.427	7.9 ± 0.9
3.189	64.8 ± 0.5	3.855	20.1 ± 1.0	4.436	69.6 ± 1.6
3.196	14.0 ± 0.9	3.861	57.9 ± 1.1	4.446	4.9 ± 0.8
3.213	1.8 ± 0.3	3.875	3.0 ± 0.4	4.455	22.1 ± 1.0
3.234	13.5 ± 0.7	3.894	2.2 ± 0.4	4.477	49.9 ± 2.1
3.242	27.8 ± 0.9	3.903	13.5 ± 0.8	4.482	32.7 ± 2.4
3.276	83.5 ± 2.0	3.910	21.4 ± 1.2	4.493	27.9 ± 1.2

Table 3. Continued

E_n (keV)	$g\Gamma_n\Gamma_\gamma/\Gamma$ (meV)	E_n (keV)	$g\Gamma_n\Gamma_\gamma/\Gamma$ (meV)	E_n (keV)	$g\Gamma_n\Gamma_\gamma/\Gamma$ (meV)
4.503	5[illegible].6 ± 1.4	5.239	27.4 ± 1.2	6.016	60.[illegible] ± 1.6
4.527	12.0 ± 0.8	5.253	44.0 ± 1.2	6.040	4.7 ± 1.1
4.540	15.3 ± 0.8	5.285	22.7 ± 1.3	6.052	23.0 ± 1.3
4.554	26.4 ± 1.1	5.296	87.5 ± 2.0	6.070	51.1 ± 1.8
4.566	5.5 ± 0.7	5.304	35.4 ± 1.8	6.083	43.6 ± 1.8
4.585	15.2 ± 0.9	5.314	40.9 ± 1.4	6.093	19.5 ± 2.1
4.609	20.1 ± 0.6	5.332	25.0 ± 1.4	6.108	34.9 ± 1.6
4.626	19.5 ± 0.6	5.343	60.9 ± 1.5	6.133	95.2 ± 2.3
4.645	35.4 ± 0.8	5.360	52.7 ± 1.4	6.165	106.3 ± 3.2
4.655	17.5 ± 0.7	5.386	6.6 ± 0.7	6.174	19.5 ± 3.1
4.674	7.6 ± 0.7	5.411	69.4 ± 1.6	6.181	49.0 ± 2.4
4.682	13.4 ± 0.7	5.430	8.6 ± 2.2	6.201	63.9 ± 2.0
4.694	54.6 ± 1.0	5.434	19.1 ± 2.2	6.223	49.9 ± 1.8
4.705	5.1 ± 0.5	5.448	12.3 ± 0.9	6.246	59.8 ± 3.0
4.716	42.5 ± 0.9	5.460	8.9 ± 0.8	6.260	3.3 ± 1.4
4.738	3.7 ± 0.5	5.476	9.2 ± 1.1	6.287	66.1 ± 2.6
4.751	60.5 ± 1.0	5.491	94.0 ± 2.7	6.306	88.6 ± 5.1
4.777	14.0 ± 0.9	5.514	58.5 ± 1.7	6.315	107.4 ± 4.5
4.786	35.2 ± 0.9	5.538	67.0 ± 1.9	6.334	7.6 ± 1.5
4.810	6.5 ± 0.5	5.562	22.3 ± 1.6	6.365	33.5 ± 2.2
4.855	21.4 ± 1.0	5.569	10.2 ± 2.0	6.386	42.6 ± 2.2
4.865	39.7 ± 1.1	5.577	65.1 ± 2.0	6.408	63.0 ± 2.8
4.877	17.5 ± 1.0	5.618	61.9 ± 1.8	6.420	36.7 ± 2.6
4.885	32.2 ± 1.1	5.639	34.7 ± 1.5	6.453	64.9 ± 4.0
4.894	9.4 ± 0.9	5.663	17.4 ± 1.2	6.488	85.4 ± 3.7
4.908	23.3 ± 1.1	5.683	26.2 ± 1.3	6.499	86.1 ± 3.7
4.916	23.1 ± 1.1	5.697	15.7 ± 1.1	6.517	18.4 ± 2.3
4.933	15.7 ± 1.1	5.719	21.9 ± 2.3	6.532	92.8 ± 5.0
4.944	54.0 ± 1.3	5.726	57.8 ± 2.4	6.556	51.2 ± 2.4
4.961	28.8 ± 1.0	5.743	14.7 ± 2.3	6.581	28.3 ± 2.9
4.976	21.2 ± 0.9	5.747	10.5 ± 3.1	6.591	66.3 ± 3.1
4.998	89.0 ± 2.9	5.755	68.3 ± 2.4	6.637	138.1 ± 4.8
5.022	49.7 ± 1.2	5.779	8.0 ± 0.8	6.657	59.2 ± 2.6
5.034	6.4 ± 0.8	5.788	5.2 ± 1.0	6.667	9.8 ± 2.1
5.058	12.6 ± 1.1	5.806	55.7 ± 1.6	6.704	163.1 ± 5.4
5.065	12.6 ± 1.1	5.816	16.3 ± 1.7	6.727	20.2 ± 2.4
5.072	13.4 ± 1.1	5.822	14.7 ± 1.7	6.740	52.3 ± 2.5
5.084	32.2 ± 1.0	5.838	22.4 ± 1.1	6.761	128.9 ± 3.7
5.099	67.1 ± 1.4	5.863	7.7 ± 0.9	6.778	14.8 ± 1.8
5.124	4.9 ± 0.6	5.877	11.5 ± 1.5	6.802	21.6 ± 2.2
5.142	10.2 ± 0.7	5.884	13.1 ± 1.2	6.814	36.6 ± 2.2
5.165	48.3 ± 1.8	5.913	11.2 ± 0.9	6.829	20.2 ± 1.8
5.174	60.0 ± 1.6	5.935	93.2 ± 3.2	6.856	71.3 ± 1.9
5.195	4.7 ± 0.8	5.962	20.5 ± 6.4	6.871	28.0 ± 1.6
5.206	64.8 ± 1.4	5.964	51.3 ± 5.9	6.882	19.7 ± 1.7
5.224	21.3 ± 1.3	5.972	16.4 ± 2.0	6.903	40.8 ± 1.6
5.232	11.0 ± 1.6	5.993	62.1 ± 1.6	6.935	68.8 ± 1.9

Table 3. Continued

E_n (keV)	$g\Gamma_n\Gamma_\gamma/\Gamma$ (meV)	E_n (keV)	$g\Gamma_n\Gamma_\gamma/\Gamma$ (meV)	E_n (keV)	$g\Gamma_n\Gamma_\gamma/\Gamma$ (meV)
6.958	37.5 ± 1.8	7.194	93.6 ± 2.6	7.435	34.8 ± 2.8
6.973	66.4 ± 1.9	7.212	3.7 ± 1.4	7.446	147.2 ± 4.0
6.995	78.9 ± 2.0	7.219	3.3 ± 1.4	7.471	141.7 ± 5.0
7.037	114.6 ± 3.5	7.234	24.3 ± 1.4	7.499	33.0 ± 2.0
7.053	38.3 ± 2.2	7.251	11.1 ± 1.2	7.515	30.4 ± 2.2
7.062	32.8 ± 2.1	7.271	65.8 ± 3.2	7.528	114.6 ± 3.3
7.084	47.6 ± 1.8	7.305	24.9 ± 2.8	7 564	57.2 ± 2.9
7.096	9.7 ± 1.4	7.315	59.4 ± 2.7	7.576	95.7 ± 3.3
7.113	5.6 ± 1.2	7.326	66.8 ± 2.8	7.607	20.3 ± 2.4
7.142	52.5 ± 2.9	7.343	6.5 ± 1.1	7.615	24.6 ± 2.4
7.167	27.9 ± 2.9	7.372	18.8 ± 1.9	7.632	13.3 ± 1.7
7.175	8.1 ± 1.6	7.385	116.5 ± 3.8	7.653	49.6 ± 2.1

[a]Resonances below 2.6 keV were not included in the present work.

[b]Statistical standard deviations determined by the least squares data fitting program. Systematic uncertainties are estimated at 3.6%.

Table 4. ^{124}Te Resonance Capture Parameters

E_n (keV)	$g\Gamma_n\Gamma_\gamma/\Gamma$ (meV)	E_n (keV)	$g\Gamma_n\Gamma_\gamma/\Gamma$ (meV)	E_n (keV)	$g\Gamma_n\Gamma_\gamma/\Gamma$ (meV)
2.668[a]	17.2 ± 0.3[b]	6.010	1.6 ± 0.5	9.958	12.0 ± 1.5
2.785	7.9 ± 0.2	6.093	68.4 ± 1.5	9.979	51.2 ± 2.4
2.830	53.9 ± 0.8	6.113	25.9 ± 0.9	10.01	10.9 ± 0.9
2.917	46.5 ± 0.8	6.201	57.8 ± 1.3	10.14	51.2 ± 2.1
2.922	53.0 ± 0.7	6.235	42.9 ± 1.0	10.16	128.8 ± 2.9
3.039	19.4 ± 0.3	6.269	84.7 ± 1.6	10.25	33.9 ± 1.3
3.122	29.0 ± 0.5	6.428	46.8 ± 1.3	10.28	68.5 ± 2.0
3.204	4.7 ± 0.2	6.587	1.2 ± 0.5	10.30	31.3 ± 2.0
3.334	45.6 ± 0.6	6.647	48.8 ± 1.9	10.47	38.7 ± 1.3
3.390	49.4 ± 0.9	6.703	73.1 ± 1.5	10.52	14.8 ± 1.2
3.398	11.1 ± 0.4	6.822	21.6 ± 0.9	10.57	25.4 ± 1.4
3.515	26.7 ± 0.5	6.918	30.2 ± 1.0	10.69	34.6 ± 2.2
3.541	38.9 ± 0.5	6.931	13.5 ± 1.1	10.71	54.9 ± 1.9
3.703	5.6 ± 0.2	6.983	34.6 ± 1.2	10.78	14.7 ± 1.9
3.793	21.4 ± 0.5	7.061	87.9 ± 1.7	10.79	47.9 ± 2.1
3.852	48.1 ± 1.0	7.111	45.5 ± 1.2	10.86	114.5 ± 2.4
3.895	2.1 ± 0.2	7.190	97.3 ± 3.9	11.01	49.6 ± 3.0
4.005	1.3 ± 0.2	7.444	45.1 ± 1.3	11.02	49.8 ± 2.8
4.022	52.6 ± 0.7	7.475	85.0 ± 2.4	11.22	23.3 ± 1.2
4.180	4.2 ± 0.2	7.547	30.6 ± 1.2	11.26	46.8 ± 1.8
4.230	49.1 ± 1.0	7.685	7.3 ± 0.8	11.29	12.1 ± 1.2
4.309	26.6 ± 0.6	7.793	59.1 ± 1.7	11.34	66.7 ± 2.1
4.360	57.7 ± 0.8	7.869	62.7 ± 2.5	11.42	33.7 ± 1.3
4.411	1.0 ± 0.2	7.975	32.3 ± 1.2	11.60	64.0 ± 1.9
4.475	41.5 ± 0.7	8.009	50.5 ± 1.5	11.68	22.7 ± 2.1
4.502	48.6 ± 0.9	8.102	92.2 ± 2.0	11.70	69.9 ± 2.7
4.513	104.2 ± 1.5	8.207	36.3 ± 1.4	11.72	29.3 ± 2.3
4.634	38.3 ± 0.7	8.342	23.1 ± 1.9	11.80	38.7 ± 1.5
4.719	21.4 ± 0.5	8.353	39.2 ± 1.8	11.85	45.0 ± 1.8
4.748	7.3 ± 0.4	8.509	78.0 ± 1.9	11.91	41.7 ± 1.5
4.774	4.5 ± 0.3	8.608	43.5 ± 1.5	11.94	5.9 ± 1.3
4.870	45.6 ± 0.7	8.717	40.0 ± 1.5	12.10	28.1 ± 1.4
4.905	51.9 ± 0.9	8.758	46.3 ± 1.6	12.13	17.3 ± 1.3
4.972	0.5 ± 0.2	8.779	159.5 ± 3.2	12.16	8.2 ± 1.1
5.049	44.4 ± 0.9	8.892	75.5 ± 2.0	12.22	4.6 ± 1.0
5.061	29.4 ± 0.6	8.981	43.9 ± 1.3	12.35	68.5 ± 2.2
5.155	59.7 ± 1.3	9.030	2.5 ± 0.7	12.45	20.8 ± 1.3
5.269	14.4 ± 0.5	9.175	30.0 ± 1.9	12.53	64.7 ± 2.1
5.409	63.7 ± 1.0	9.189	45.7 ± 1.9	12.62	58.3 ± 3.3
5.474	38.9 ± 0.8	9.274	101.7 ± 3.2	12.64	89.3 ± 3.0
5.553	8.8 ± 0.4	9.473	67.0 ± 1.9	12.71	45.1 ± 1.8
5.596	47.4 ± 1.2	9.495	42.0 ± 1.6	12.74	51.6 ± 3.5
5.705	37.2 ± 0.9	9.583	79.0 ± 2.0	12.76	68.8 ± 2.7
5.750	56.7 ± 1.3	9.660	81.4 ± 1.8	12.89	91.7 ± 2.7
5.844	8.2 ± 0.6	9.696	32.4 ± 1.3	12.99	47.2 ± 1.8
5.866	39.4 ± 1.0	9.761	138.7 ± 3.4	13.06	82.6 ± 2.7
5.886	1.8 ± 0.5	9.918	56.5 ± 1.7	13.18	31.7 ± 1.6

Table 4. Continued

E_n (keV)	$g\Gamma_n\Gamma_\gamma/\Gamma$ (meV)	E_n (keV)	$g\Gamma_n\Gamma_\gamma/\Gamma$ (meV)	E_n (keV)	$g\Gamma_n\Gamma_\gamma/\Gamma$ (meV)
13.26	76.6 ± 2.8	17.51	82.2 ± 4.2	21.38	155.3 ± 6.5
13.41	70.7 ± 2.3	17.56	100.3 ± 4.3	21.65	62.7 ± 5.8
13.48	7.2 ± 2.3	17.65	31.3 ± 5.8	21.69	136.3 ± 6.1
13.50	41.0 ± 2.3	17.67	133.7 ± 6.3	21.79	170.8 ± 6.4
13.55	109.9 ± 6.8	17.74	104.1 ± 4.2	21.92	47.6 ± 4.7
13.60	253.4 ± 7.0	17.86	45.4 ± 4.9	22.00	91.2 ± 6.3
13.82	44.7 ± 2.2	17.89	62.2 ± 4.1	22.03	38.8 ± 7.0
13.87	95.1 ± 2.8	18.02	9.0 ± 3.0	22.09	54.8 ± 5.7
13.94	57.6 ± 2.4	18.05	125.6 ± 5.2	22.13	42.7 ± 4.7
14.03	37.3 ± 2.1	18.18	76.4 ± 3.5	22.23	54.9 ± 4.4
14.10	87.2 ± 2.8	18.24	123.0 ± 4.1	22.31	48.5 ± 4.0
14.20	56.2 ± 2.3	18.28	35.5 ± 2.8	22.38	111.6 ± 5.1
14.34	70.3 ± 2.7	18.36	130.4 ± 4.5	22.46	118.9 ± 5.5
14.42	52.2 ± 2.1	18.41	87.6 ± 4.1	22.52	44.1 ± 4.2
14.50	109.0 ± 3.1	18.61	33.3 ± 2.7	22.63	57.8 ± 4.4
14.63	52.8 ± 2.5	18.66	51.8 ± 4.5	22.76	168.1 ± 6.3
14.70	50.2 ± 2.2	18.70	105.0 ± 4.2	22.84	97.1 ± 5.0
14.79	5.9 ± 1.7	18.76	20.7 ± 2.4	22.98	216.3 ± 9.3
14.84	75.1 ± 2.7	18.84	10.0 ± 3.0	23.04	138.6 ± 6.0
14.91	43.3 ± 1.9	18.87	66.0 ± 3.6	23.19	10.1 ± 3.8
15.02	108.1 ± 3.0	18.91	43.8 ± 3.2	23.25	91.1 ± 5.1
15.09	36.5 ± 2.1	18.97	170.2 ± 5.0	23.40	40.7 ± 5.7
15.12	95.0 ± 3.1	19.04	57.3 ± 3.2	23.43	23.0 ± 6.8
15.24	81.4 ± 2.9	19.09	10.0 ± 2.2	23.47	94.9 ± 5.8
15.32	56.1 ± 2.9	19.26	71.3 ± 3.4	23.54	85.0 ± 5.2
15.35	41.4 ± 2.5	19.34	99.0 ± 5.3	23.68	32.0 ± 4.0
15.44	156.6 ± 4.8	19.43	116.5 ± 4.9	23.77	10.0 ± 4.1
15.57	28.6 ± 3.7	19.52	161.1 ± 6.0	23.82	38.5 ± 4.1
15.59	155.5 ± 5.3	19.61	47.7 ± 3.5	23.92	123.9 ± 6.1
15.70	8.1 ± 1.6	19.71	64.9 ± 4.1	23.99	81.5 ± 5.4
15.81	49.1 ± 2.9	19.89	171.2 ± 6.6	24.39	166.6 ± 8.8
15.91	119.6 ± 4.3	19.98	174.6 ± 5.9	24.51	50.6 ± 5.0
16.08	85.7 ± 3.9	20.05	106.2 ± 4.8	24.59	211.1 ± 8.9
16.16	105.9 ± 4.2	20.20	52.0 ± 3.9	24.67	159.4 ± 10.6
16.27	85.1 ± 3.6	20.26	44.4 ± 3.5	24.78	119.0 ± 8.8
16.33	79.7 ± 4.0	20.41	81.7 ± 4.5	24.83	194.0 ± 9.1
16.48	69.0 ± 5.5	20.58	84.1 ± 5.1	24.98	41.4 ± 9.7
16.50	82.8 ± 5.1	20.63	101.4 ± 4.8	25.01	117.0 ± 9.1
16.75	44.4 ± 3.0	20.72	53.5 ± 4.2	25.15	88.3 ± 11.9
16.81	28.8 ± 2.7	20.75	28.0 ± 3.9	25.18	182.3 ± 12.8
16.86	136.3 ± 4.6	20.83	16.1 ± 2.9	25.26	31.3 ± 4.9
17.00	124.5 ± 4.3	20.94	47.9 ± 4.0	25.39	120.0 ± 5.9
17.07	57.2 ± 4.7	21.10	107.2 ± 4.9	25.44	55.1 ± 5.9
17.09	118.3 ± 4.6	21.16	80.7 ± 4.8	25.49	111.9 ± 6.0
17.24	44.9 ± 2.8	21.23	80.8 ± 4.5	25.74	29.1 ± 3.9
17.33	44.9 ± 2.8	21.28	45.2 ± 4.3	25.86	54.0 ± 4.0
17.47	55.5 ± 4.1	21.32	137.4 ± 5.7	25.94	126.5 ± 5.5

Table 4. Continued.

E_n (keV)	$g\Gamma_n\Gamma_\gamma/\Gamma$ (meV)	E_n (keV)	$g\Gamma_n\Gamma_\gamma/\Gamma$ (meV)	E_n (keV)	$g\Gamma_n\Gamma_\gamma/\Gamma$ (meV)
26.06	57.1 ± 5.5	30.28	205.8 ± 9.5	35.53	86.2 ± 12.3
26.11	100.7 ± 5.5	30.53	72.9 ± 6.7	35.58	92.0 ± 10.5
26.25	66.1 ± 6.2	30.61	51.8 ± 6.3	35.68	37.8 ± 7.5
26.30	128.9 ± 6.3	30.70	132.6 ± 7.9	35.80	128.6 ± 9.1
26.52	231.1 ± 9.4	30.83	101.4 ± 7.6	35.94	172.8 ± 12.9
26.59	50.7 ± 5.6	30.93	131.9 ± 7.7	36.05	15.2 ± 7.5
26.71	63.7 ± 6.7	31.00	52.8 ± 6.4	36.22	124.4 ± 9.2
26.76	133.3 ± 7.0	31.11	117.0 ± 7.7	36.35	61.9 ± 8.1
26.86	114.8 ± 6.0	31.27	145.7 ± 8.6	36.47	134.3 ± 10.0
27.10	37.7 ± 6.5	31.51	39.0 ± 7.1	36.61	33.6 ± 9.8
27.16	125.8 ± 7.1	31.61	82.7 ± 11.6	36.67	60.3 ± 9.0
27.25	33.1 ± 5.0	31.67	146.6 ± 10.1	36.74	56.0 ± 9.0
27.32	22.2 ± 5.1	31.75	42.2 ± 7.1	36.91	191.2 ± 10.8
27.42	62.1 ± 6.4	31.83	134.4 ± 8.9	37.17	180.8 ± 10.3
27.49	130.3 ± 7.6	31.90	59.6 ± 8.4	37.27	93.0 ± 9.2
27.57	166.7 ± 8.3	32.04	86.8 ± 10.5	37.34	62.5 ± 9.1
27.63	113.8 ± 8.6	32.11	213.3 ± 14.3	37.40	22.3 ± 9.7
27.69	38.5 ± 7.0	32.24	104.9 ± 11.8	37.51	143.0 ± 9.5
27.78	85.9 ± 6.0	32.31	115.8 ± 9.2	37.72	65.9 ± 8.4
27.84	93.1 ± 7.0	32.46	106.1 ± 8.5	37.80	127.1 ± 9.6
27.96	107.0 ± 10.1	32.60	23.8 ± 11.3	37.97	64.7 ± 9.2
28.00	128.4 ± 9.2	32.65	145.4 ± 10.9	38.08	225.5 ± 13.3
28.10	35.8 ± 5.4	32.79	172.6 ± 15.2	38.19	138.0 ± 13.6
28.19	35.8 ± 5.7	32.96	201.4 ± 11.4	38.26	136.7 ± 10.4
28.26	26.6 ± 6.0	33.14	149.0 ± 10.6	38.42	62.4 ± 8.6
28.35	78.6 ± 5.8	33.20	83.0 ± 11.2	38.53	103.9 ± 9.3
28.42	64.6 ± 5.4	33.39	232.7 ± 13.3	38.64	155.8 ± 11.0
28.51	105.2 ± 6.2	33.49	40.8 ± 7.0	38.71	180.0 ± 11.1
28.67	149.0 ± 6.6	33.64	210.2 ± 11.4	38.83	46.7 ± 7.9
28.77	117.6 ± 6.8	33.76	10.0 ± 6.1	39.05	39.2 ± 16.3
28.83	75.6 ± 7.8	33.86	27.1 ± 8.4	39.13	399.2 ± 20.6
28.91	58.5 ± 7.4	33.92	163.3 ± 9.7	39.29	72.8 ± 15.5
28.96	86.3 ± 6.4	34.01	170.5 ± 9.6	39.35	85.1 ± 12.1
29.11	65.3 ± 7.1	34.08	150.7 ± 9.5	39.49	146.3 ± 11.0
29.17	243.1 ± 9.3	34.30	156.8 ± 9.7	39.64	293.5 ± 16.4
29.22	61.8 ± 8.2	34.40	85.4 ± 7.8	39.74	147.9 ± 11.9
29.32	80.7 ± 7.4	34.48	19.0 ± 6.5	39.91	269.1 ± 13.3
29.38	146.5 ± 7.7	34.58	210.8 ± 10.0	40.08	95.8 ± 10.7
29.46	46.9 ± 5.2	34.73	118.6 ± 8.5	40.24	36.4 ± 11.4
29.67	136.8 ± 7.2	34.88	98.5 ± 8.1	40.32	186.1 ± 11.6
29.78	158.2 ± 8.4	35.02	54.5 ± 8.9	40.46	115.2 ± 10.4
29.90	90.7 ± 6.4	35.08	120.9 ± 9.0	40.58	135.7 ± 11.3
30.03	156.9 ± 8.2	35.24	114.5 ± 9.6	40.77	285.4 ± 17.3
30.16	122.5 ± 7.9	35.32	157.8 ± 10.3	40.99	202.2 ± 12.3
30.23	47.6 ± 7.8	35.41	172.6 ± 10.2	41.10	82.9 ± 9.6

[a]Resonances below 2.6 keV were not included in the present work.

[b]Statistical standard deviations determined by the least squares data fitting program. Systematic uncertainties are estimated at 3.6%.

Table 5. ^{125}Te Resonance Capture Parameters

E_n (keV)	$g\Gamma_n\Gamma_\gamma/\Gamma$ (meV)	E_n (keV)	$g\Gamma_n\Gamma_\gamma/\Gamma$ (meV)	E_n (keV)	$g\Gamma_n\Gamma_\gamma/\Gamma$ (meV)
2.659[a]	9.2 ± 0.3[b]	3.623	4.3 ± 0.5	4.597	51.6 ± 1.7
2.673	9.6 ± 0.3	3.629	29.4 ± 0.7	4.600	54.3 ± 0.1
2.701	0.7 ± 0.1	3.647	18.3 ± 0.7	4.633	4.8 ± 0.6
2.740	62.7 ± 1.6	3.653	18.3 ± 0.6	4.641	11.0 ± 0.6
2.755	2.2 ± 0.2	3.697	32.8 ± 0.7	4.693	49.2 ± 1.0
2.763	1.7 ± 0.1	3.704	4.7 ± 0.4	4.707	6.8 ± 0.5
2.788	42.5 ± 0.6	3.726	9.5 ± 0.4	4.721	11.8 ± 0.6
2.793	7.0 ± 0.5	3.743	32.2 ± 0.7	4.796	32.1 ± 0.9
2.811	3.0 ± 0.2	3.774	1.1 ± 0.2	4.806	24.1 ± 0.9
2.846	85.3 ± 1.4	3.791	9.1 ± 0.5	4.838	5.1 ± 0.6
2.887	2.0 ± 0.2	3.816	3.7 ± 0.6	4.848	23.0 ± 1.4
2.910	9.3 ± 0.3	3.822	61.0 ± 1.1	4.855	57.3 ± 1.6
2.921	32.6 ± 0.5	3.841	4.4 ± 0.5	4.878	8.5 ± 1.0
2.938	11.6 ± 0.3	3.847	16.4 ± 0.6	4.884	18.4 ± 1.1
2.977	10.1 ± 0.3	3.859	22.4 ± 0.6	4.927	38.5 ± 1.2
2.993	36.4 ± 0.5	3.877	42.6 ± 0.9	4.935	2.1 ± 0.8
3.005	10.0 ± 0.5	3.925	22.9 ± 0.7	4.951	13.0 ± 0.7
3.009	10.2 ± 0.4	3.959	9.0 ± 0.5	4.972	68.7 ± 1.6
3.029	2.6 ± 0.2	3.988	20.1 ± 0.7	4.988	38.8 ± 1.3
3.046	10.2 ± 0.3	4.008	73.0 ± 1.5	5.073	23.4 ± 0.9
3.058	2.4 ± 0.2	4.014	9.6 ± 0.9	5.082	6.3 ± 0.7
3.098	31.0 ± 0.5	4.033	1.6 ± 0.3	5.096	0.4 ± 0.4
3.122	51.0 ± 0.7	4.056	60.9 ± 1.1	5.123	10.1 ± 0.6
3.131	2.1 ± 0.2	4.086	51.7 ± 1.1	5.158	20.1 ± 1.6
3.144	9.0 ± 0.3	4.095	3.4 ± 0.5	5.163	20.0 ± 1.4
3.158	34.4 ± 0.6	4.116	33.5 ± 1.0	5.181	31.2 ± 1.2
3.181	49.1 ± 0.6	4.123	25.5 ± 1.2	5.206	5.4 ± 0.7
3.201	2.2 ± 0.2	4.130	18.7 ± 2.7	5.216	41.9 ± 1.4
3.211	1.6 ± 0.2	4.133	26.4 ± 2.5	5.244	16.3 ± 0.8
3.236	19.5 ± 0.5	4.183	23.7 ± 0.7	5.256	6.4 ± 0.7
3.283	13.4 ± 0.4	4.196	2.8 ± 0.4	5.287	3.5 ± 0.4
3.296	6.1 ± 0.7	4.226	7.7 ± 0.4	5.309	27.3 ± 1.9
3.301	71.0 ± 1.1	4.247	56.0 ± 1.0	5.314	52.4 ± 2.0
3.324	9.9 ± 0.4	4.271	5.2 ± 0.6	5.345	2.0 ± 0.3
3.336	2.9 ± 0.2	4.277	9.9 ± 0.6	5.370	3.9 ± 0.4
3.396	62.3 ± 1.0	4.307	14.1 ± 0.5	5.386	11.1 ± 0.6
3.402	8.4 ± 0.6	4.319	23.4 ± 0.9	5.433	34.6 ± 2.0
3.439	88.7 ± 1.1	4.326	22.0 ± 0.8	5.438	41.9 ± 2.2
3.451	1.5 ± 0.2	4.358	2.7 ± 0.3	5.451	16.7 ± 0.7
3.460	12.0 ± 0.4	4.400	2.9 ± 0.3	5.486	46.3 ± 1.3
3.487	9.8 ± 0.4	4.427	40.3 ± 1.4	5.501	13.5 ± 0.7
3.503	7.8 ± 0.3	4.433	36.7 ± 1.2	5.538	34.0 ± 1.0
3.519	4.2 ± 0.3	4.456	1.3 ± 0.2	5.553	26.6 ± 0.9
3.542	10.9 ± 0.4	4.488	7.3 ± 0.4	5.569	20.1 ± 1.2
3.573	10.5 ± 0.4	4.503	11.7 ± 0.5	5.577	16.1 ± 1.0
3.585	62.5 ± 0.9	4.560	9.9 ± 0.6	5.602	22.5 ± 0.8
3.614	1.3 ± 0.2	4.567	1.2 ± 0.4	5.630	3.7 ± 0.4

Table 5. Continued

E_n (keV)	$g\Gamma_n\Gamma_\gamma/\Gamma$ (meV)	E_n (keV)	$g\Gamma_n\Gamma_\gamma/\Gamma$ (meV)	E_n (keV)	$g\Gamma_n\Gamma_\gamma/\Gamma$ (meV)
5.647	11.7 ± 0.8	6.345	15.1 ± 0.9	7.034	59.3 ± 2.0
5.658	35.7 ± 1.4	6.367	19.9 ± 1.2	7.069	40.4 ± 1.7
5.666	38.9 ± 1.3	6.384	53.7 ± 1.6	7.088	23.1 ± 1.4
5.681	9.1 ± 0.6	6.446	26.9 ± 1.8	7.107	108.0 ± 2.8
5.700	23.2 ± 1.3	6.454	57.5 ± 2.1	7.138	16.7 ± 1.2
5.706	62.2 ± 1.6	6.482	21.1 ± 2.0	7.164	64.0 ± 1.9
5.753	4.1 ± 0.7	6.490	32.5 ± 2.1	7.196	2.1 ± 0.8
5.761	28.3 ± 1.0	6.502	57.3 ± 1.8	7.227	49.9 ± 2.2
5.800	20.5 ± 0.7	6.517	23.0 ± 1.3	7.240	46.7 ± 2.2
5.824	37.4 ± 0.9	6.533	24.4 ± 1.2	7.252	26.2 ± 1.8
5.853	6.7 ± 0.5	6.571	1.9 ± 0.4	7.277	76.6 ± 2.3
5.876	40.0 ± 1.0	6.588	5.2 ± 0.6	7.301	23.9 ± 2.1
5.888	16.1 ± 0.9	6.600	3.1 ± 0.5	7.313	17.4 ± 1.5
5.906	2.5 ± 0.5	6.620	2.4 ± 0.4	7.338	47.1 ± 2.0
5.930	51.9 ± 1.5	6.646	14.1 ± 0.8	7.365	13.9 ± 1.6
5.963	36.6 ± 1.4	6.656	45.4 ± 1.0	7.376	34.9 ± 2.0
5.979	4.0 ± 0.7	6.680	29.9 ± 0.9	7.400	73.0 ± 2.2
6.022	19.4 ± 1.1	6.707	53.2 ± 1.1	7.427	41.0 ± 1.9
6.036	18.2 ± 1.0	6.728	20.7 ± 0.7	7.448	4.5 ± 1.0
6.055	20.7 ± 1.0	6.778	13.1 ± 1.4	7.469	56.6 ± 1.9
6.086	39.4 ± 2.0	6.788	68.2 ± 0.1	7.504	38.8 ± 1.7
6.092	24.5 ± 2.0	6.791	72.2 ± 2.6	7.526	37.0 ± 1.9
6.105	8.4 ± 1.1	6.839	24.3 ± 2.2	7.600	60.5 ± 1.6
6.114	7.6 ± 0.9	6.846	43.8 ± 2.1	7.616	48.6 ± 1.6
6.135	3.6 ± 0.6	6.875	10.7 ± 1.1	7.638	58.4 ± 1.4
6.176	29.9 ± 1.5	6.890	59.1 ± 1.6	7.667	5.5 ± 0.8
6.188	76.8 ± 2.2	6.914	25.1 ± 2.2	7.680	13.2 ± 0.9
6.239	1.8 ± 0.5	6.922	57.7 ± 2.6	7.712	26.0 ± 1.1
6.262	24.1 ± 1.0	6.948	19.4 ± 1.0	7.743	42.1 ± 2.0
6.280	8.4 ± 0.7	6.979	18.0 ± 1.3	7.750	75.0 ± 0 1
6.310	46.9 ± 1.5	7.000	39.9 ± 1.6	7.758	68.5 ± 2.5
6.328	20.2 ± 1.0	7.018	60.1 ± 2.0	7.774	10.3 ± 1.2

[a]Resonances below 2.6 keV were not included in the present work.

[b]Statistical standard deviations determined by the least squares data fitting program. Systematic uncertainties are estimated at 3.6%.

Table 6. ^{126}Te Resonance Capture Parameters

E_n (keV)	$g\Gamma_n\Gamma_\gamma/\Gamma$ (meV)	E_n (keV)	$g\Gamma_n\Gamma_\gamma/\Gamma$ (meV)	E_n (keV)	$g\Gamma_n\Gamma_\gamma/\Gamma$ (meV)
2.712[a]	6.3 ± 0.2[b]	10.98	134.5 ± 3.5	17.73	53.6 ± 3.3
2.940	44.0 ± 0.7	11.00	50.5 ± 3.0	17.78	78.8 ± 3.8
3.198	27.4 ± 0.5	11.18	116.3 ± 2.9	18.06	41.6 ± 2.5
3.288	29.1 ± 0.5	11.26	36.1 ± 1.5	18.22	156.8 ± 4.6
3.682	22.2 ± 0.4	11.77	87.6 ± 2.1	18.35	107.9 ± 4.2
3.770	1.4 ± 0.2	11.85	135.5 ± 3.5	18.66	111.6 ± 5.0
3.782	33.3 ± 0.5	11.93	40.3 ± 1.7	18.81	86.9 ± 4.9
4.006	7.5 ± 0.3	12.02	97.4 ± 5.1	18.87	44.5 ± 4.2
4.211	24.0 ± 0.5	12.03	119.1 ± 4.3	18.93	222.3 ± 8.5
4.287	10.1 ± 0.4	12.23	43.2 ± 2.2	19.34	30.9 ± 2.7
4.566	60.8 ± 3.0	12.50	37.8 ± 2.1	19.51	63.4 ± 4.1
4.670	34.4 ± 0.6	12.74	43.5 ± 2.1	19.57	165.3 ± 6.8
5.111	71.1 ± 1.2	12.84	96.1 ± 3.3	19.75	45.1 ± 3.2
5.158	93.5 ± 1.3	12.99	32.5 ± 2.1	19.84	110.0 ± 5.2
5.327	39.1 ± 0.8	13.17	38.2 ± 2.0	19.89	49.3 ± 4.0
5.484	37.1 ± 1.0	13.44	76.2 ± 3.0	20.07	50.1 ± 3.7
5.514	8.8 ± 0.5	13.48	37.2 ± 2.5	20.30	88.4 ± 5.1
5.570	4.0 ± 0.4	13.61	83.6 ± 3.3	20.61	150.4 ± 8.7
5.753	65.8 ± 1.4	13.84	51.3 ± 2.6	21.00	194.4 ± 8.1
5.945	5.5 ± 0.6	13.88	43.7 ± 2.2	21.16	141.2 ± 6.2
5.970	62.6 ± 1.9	13.94	59.9 ± 2.8	21.36	40.4 ± 3.7
6.399	43.0 ± 1.3	14.02	86.7 ± 3.6	21.68	28.3 ± 3.1
6.580	80.0 ± 1.6	14.12	100.5 ± 3.4	21.75	34.7 ± 3.0
6.759	38.5 ± 1.0	14.49	130.7 ± 3.7	21.83	94.1 ± 4.5
6.843	98.9 ± 1.5	14.56	64.1 ± 3.1	21.95	180.0 ± 7.9
7.222	12.3 ± 0.7	14.67	122.5 ± 4.1	22.23	126.1 ± 5.4
7.268	136.8 ± 2.3	15.19	259.2 ± 6.1	22.37	70.0 ± 4.0
7.397	34.6 ± 1.5	15.25	74.3 ± 3.5	22.62	118.8 ± 5.2
7.409	43.0 ± 1.5	15.35	45.0 ± 2.5	22.82	23.7 ± 2.8
7.774	174.4 ± 2.6	15.85	168.1 ± 5.3	22.96	20.5 ± 3.2
7.866	41.4 ± 1.2	15.90	39.0 ± 3.4	23.16	330.1 ± 9.6
8.133	29.9 ± 1.0	15.93	153.3 ± 5.3	23.23	145.3 ± 6.5
8.359	3.2 ± 0.5	16.04	56.0 ± 3.5	23.26	44.0 ± 6.6
8.409	39.6 ± 1.3	16.17	181.0 ± 5.8	23.70	42.6 ± 4.3
8.474	89.9 ± 1.8	16.24	30.5 ± 2.3	23.76	44.0 ± 3.6
8.696	66.4 ± 1.7	16.29	103.3 ± 4.6	23.89	155.2 ± 6.6
8.868	45.2 ± 1.4	16.39	64.2 ± 3.6	23.97	134.7 ± 5.8
9.033	10.9 ± 1.0	16.50	79.6 ± 3.2	24.16	41.9 ± 4.7
9.055	57.6 ± 1.6	16.61	128.9 ± 4.2	24.21	47.4 ± 4.7
9.283	44.0 ± 1.5	16.69	38.2 ± 2.4	24.66	203.7 ± 7.9
9.625	104.5 ± 2.6	16.77	60.2 ± 3.2	24.80	17.4 ± 4.8
9.648	33.1 ± 1.4	16.99	60.5 ± 3.1	24.84	45.5 ± 4.7
9.964	85.8 ± 2.1	17.10	49.0 ± 3.5	24.95	195.4 ± 8.1
10.16	25.2 ± 1.3	17.15	9.9 ± 2.1	25.01	90.2 ± 6.8
10.50	42.9 ± 1.6	17.58	150.3 ± 5.3	25.27	43.2 ± 4.4
10.57	241.7 ± 4.5	17.62	245.9 ± 6.7	25.41	136.9 ± 7.5
10.61	102.1 ± 3.0	17.67	140.9 ± 4.9	25.64	149.8 ± 8.0

Table 6. Continued

E_n (keV)	$g\Gamma_n\Gamma_\gamma/\Gamma$ (meV)	E_n (keV)	$g\Gamma_n\Gamma_\gamma/\Gamma$ (meV)	E_n (keV)	$g\Gamma_n\Gamma_\gamma/\Gamma$ (meV)
25.74	21.2 ± 4.1	32.99	47.2 ± 6.9	40.69	83.4 ± 8.0
25.84	124.0 ± 7.1	33.14	151.7 ± 8.4	40.78	57.2 ± 8.2
26.28	64.1 ± 5.7	33.53	209.0 ± 10.6	41.00	45.6 ± 7.1
26.35	40.9 ± 4.6	33.92	86.6 ± 7.3	41.13	36.8 ± 11.4
26.49	93.8 ± 6.1	34.01	109.8 ± 8.4	41.20	74.6 ± 9.4
26.71	141.5 ± 7.6	34.33	125.8 ± 8.8	41.31	38.6 ± 7.3
26.83	195.1 ± 10.5	34.58	24.7 ± 6.0	41.46	76.9 ± 8.9
26.98	11.6 ± 7.6	34.68	140.3 ± 9.3	41.69	31.6 ± 13.6
27.03	206.0 ± 11.8	34.93	52.5 ± 9.1	41.75	146.3 ± 13.4
27.10	48.6 ± 7.0	35.01	112.2 ± 9.1	41.88	54.8 ± 9.2
27.26	16.1 ± 5.3	35.15	64.7 ± 6.9	41.97	120.2 ± 9.4
27.37	113.1 ± 12.8	35.29	86.8 ± 7.5	42.09	26.1 ± 7.6
27.41	183.3 ± 12.3	35.46	18.2 ± 6.6	42.53	53.3 ± 12.8
27.71	150.6 ± 9.6	35.56	29.6 ± 9.1	42.59	133.6 ± 11.1
27.98	161.9 ± 8.7	35.61	32.4 ± 6.8	42.74	17.9 ± 6.5
28.23	35.6 ± 8.6	35.75	59.7 ± 7.2	42.84	37.8 ± 7.6
28.29	270.4 ± 12.8	36.05	48.7 ± 12.6	42.97	74.9 ± 11.7
28.39	134.2 ± 8.5	36.10	119.2 ± 11.4	43.04	125.4 ± 10.5
28.50	85.3 ± 7.6	36.22	23.4 ± 6.7	43.19	151.2 ± 9.8
28.66	43.0 ± 5.7	36.39	48.2 ± 10.0	43.47	141.5 ± 8.8
28.88	28.2 ± 5.0	36.46	178.7 ± 10.8	43.70	120.1 ± 8.9
29.07	69.6 ± 11.2	36.56	97.6 ± 7.8	43.92	55.8 ± 16.6
29.11	117.3 ± 11.2	36.69	121.3 ± 9.4	43.98	210.1 ± 16.7
29.44	160.9 ± 9.9	36.92	45.4 ± 6.5	44.05	65.3 ± 13.0
29.49	137.2 ± 10.7	37.00	63.7 ± 7.8	44.32	133.2 ± 10.2
29.73	17.3 ± 4.6	37.11	58.5 ± 7.3	44.42	53.9 ± 8.9
30.07	150.5 ± 13.8	37.26	88.3 ± 8.3	44.66	185.4 ± 11.1
30.11	154.5 ± 11.4	37.36	42.3 ± 5.8	44.93	58.3 ± 8.5
30.23	16.7 ± 5.9	37.54	50.3 ± 7.6	45.03	30.1 ± 8.7
30.31	99.5 ± 8.6	37.63	116.8 ± 8.8	45.17	38.3 ± 8.4
30.38	160.1 ± 9.0	37.73	24.5 ± 6.8	45.60	250.5 ± 13.8
30.58	172.3 ± 9.0	37.87	47.0 ± 6.0	45.71	164.1 ± 11.6
30.93	46.2 ± 5.7	37.97	83.5 ± 7.5	46.10	102.3 ± 15.0
31.08	59.5 ± 7.1	38.13	106.4 ± 8.6	46.18	172.2 ± 13.0
31.24	114.4 ± 8.2	38.26	70.6 ± 6.9	46.48	31.9 ± 8.9
31.47	43.4 ± 9.4	38.56	98.0 ± 12.6	46.67	166.1 ± 12.6
31.51	100.5 ± 9.1	38.62	103.4 ± 9.5	46.76	41.7 ± 10.9
31.63	54.5 ± 6.8	38.83	32.0 ± 11.3	46.87	104.1 ± 10.4
31.68	10.0 ± 6.9	38.89	166.3 ± 10.9	47.12	102.0 ± 9.7
31.81	140.1 ± 8.3	39.20	100.0 ± 7.5	47.26	164.0 ± 11.4
31.98	135.4 ± 10.2	39.43	178.1 ± 10.6	47.40	97.3 ± 9.9
32.02	31.6 ± 10.3	39.65	87.1 ± 10.0	47.54	45.0 ± 9.4
32.17	164.2 ± 8.6	39.73	168.9 ± 9.7	47.89	155.6 ± 12.2
32.25	44.1 ± 5.7	40.01	93.0 ± 9.2	48.03	76.4 ± 10.8
32.55	32.6 ± 7.2	40.31	42.8 ± 12.0	48.39	129.7 ± 12.4
32.62	184.3 ± 8.9	40.38	190.6 ± 12.4	48.76	154.1 ± 12.9
32.91	197.8 ± 9.7	40.53	155.3 ± 11.1	48.94	189.0 ± 12.4

Table 6. Continued

E_n (keV)	$g\Gamma_n\Gamma_\gamma/\Gamma$ (meV)	E_n (keV)	$g\Gamma_n\Gamma_\gamma/\Gamma$ (meV)	E_n (keV)	$g\Gamma_n\Gamma_\gamma/\Gamma$ (meV)
49.20	301.5 ± 15.2	51.59	84.9 ± 11.5	53.41	296.6 ± 17.9
49.39	26.7 ± 10.9	51.86	430.2 ± 19.7	53.65	178.7 ± 15.9
49.55	294.9 ± 15.3	52.21	184.6 ± 15.8	54.02	411.9 ± 33.0
50.13	211.3 ± 13.8	52.36	166.9 ± 14.3	54.32	226.6 ± 17.2
50.30	146.2 ± 13.8	52.52	68.0 ± 18.2	54.58	82.8 ± 18.6
50.59	31.4 ± 10.1	52.60	178.0 ± 17.6	54.67	163.6 ± 15.7
50.79	40.8 ± 10.6	52.81	131.5 ± 13.8	54.86	125.7 ± 13.6
51.01	73.6 ± 11.6	53.10	168.2 ± 15.7	55.04	96.1 ± 13.4
51.15	64.4 ± 11.2	53.29	202.1 ± 18.0	55.18	35.1 ± 13.5

[a]Resonances below 2.6 keV were not included in the present work.

[b]Statistical standard deviations determined by the least squares data fitting program. Systematic uncertainties are estimated at 3.6%.

Table 7. Total Resonance Widths

E_n (keV)	Γ (eV)
^{122}Te	
2.868	1.06 ± 0.02
2.968	0.75 ± 0.01
3.190	1.55 ± 0.03
3.486	1.02 ± 0.03
3.705	0.87 ± 0.02
3.993	0.80 ± 0.02
4.214	1.02 ± 0.05
4.280	1.16 ± 0.03
4.448	0.82 ± 0.03
4.767	2.06 ± 0.06
4.854	1.86 ± 0.07
5.011	3.39 ± 0.13
5.335	3.40 ± 0.12
5.482	6.23 ± 0.29
5.791	2.58 ± 0.10
6.131	2.40 ± 0.12
6.246	3.67 ± 0.26
6.536	3.43 ± 0.21
7.059	2.10 ± 0.16
7.873	16.00 ± 2.00
8.180	2.43 ± 0.14
8.277	1.96 ± 0.10
9.235	3.12 ± 0.19
9.797	6.27 ± 0.36
10.45	8.19 ± 0.34
10.60	3.18 ± 0.13
10.82	6.18 ± 0.23
10.99	5.16 ± 0.29
11.74	4.33 ± 0.24
13.05	4.16 ± 0.25
14.34	5.88 ± 0.30
14.63	5.28 ± 0.20
14.70	10.80 ± 0.59
14.98	9.43 ± 0.46
15.10	14.50 ± 1.10
15.17	7.25 ± 0.59
15.55	7.58 ± 0.41
16.10	5.16 ± 0.25
16.43	11.20 ± 1.10
16.56	12.30 ± 0.73
16.74	6.67 ± 0.42
17.18	6.27 ± 0.49
17.46	16.70 ± 2.10
^{122}Te cont.	
17.61	9.48 ± 1.00
17.89	15.10 ± 0.84
17.96	8.38 ± 1.10
18.17	10.10 ± 0.87
18.35	14.90 ± 1.30
18.54	7.38 ± 0.69
18.71	9.09 ± 0.45
18.84	12.50 ± 0.75
18.91	26.40 ± 2.50
19.05	13.80 ± 0.94
19.19	19.80 ± 1.70
19.51	14.70 ± 1.60
19.72	34.70 ± 10.00
20.00	12.60 ± 0.55
^{123}Te	
2.672	0.41 ± 0.01
2.871	0.95 ± 0.03
2.948	0.63 ± 0.01
3.057	1.07 ± 0.04
3.276	1.32 ± 0.04
3.502	1.37 ± 0.04
3.692	3.57 ± 0.11
3.835	2.64 ± 0.15
4.998	2.08 ± 0.09
5.491	2.43 ± 0.09
5.935	2.69 ± 0.13
6.246	4.34 ± 0.35
6.453	2.87 ± 0.22
6.532	2.72 ± 0.19
6.637	3.94 ± 0.18
6.704	5.51 ± 0.27
7.037	2.84 ± 0.11
7.142	5.37 ± 0.46
7.271	4.14 ± 0.30
7.305	4.04 ± 0.53
7.385	4.61 ± 0.23
7.471	9.71 ± 0.61
^{124}Te	
2.830	1.70 ± 0.03
3.390	0.80 ± 0.02
3.852	3.38 ± 0.10
4.230	2.09 ± 0.06
5.155	0.65 ± 0.01
5.596	2.65 ± 0.09
6.647	3.71 ± 0.22
7.190	2.98 ± 0.18
7.475	1.98 ± 0.06
7.869	2.54 ± 0.12
9.274	2.73 ± 0.10
9.979	3.75 ± 0.24
13.55	3.58 ± 0.29
13.60	3.04 ± 0.09
17.47	8.75 ± 0.89
22.98	10.90 ± 0.60
24.39	13.80 ± 1.10
24.67	9.20 ± 0.78
26.52	21.10 ± 1.40
32.11	27.80 ± 3.00
32.79	48.10 ± 6.40
35.94	30.40 ± 3.20
38.08	33.10 ± 3.10
39.13	40.80 ± 3.30
39.64	36.60 ± 3.20
40.77	28.20 ± 2.40
^{125}Te	
2.740	0.74 ± 0.02
2.846	0.99 ± 0.02
^{126}Te	
2.940	2.53 ± 0.05
4.566	0.96 ± 0.05
5.484	1.28 ± 0.04
5.970	3.27 ± 0.14
17.10	8.92 ± 0.83
18.93	14.70 ± 0.83
20.61	10.10 ± 0.87
21.95	18.30 ± 1.20
54.02	109. ± 12.

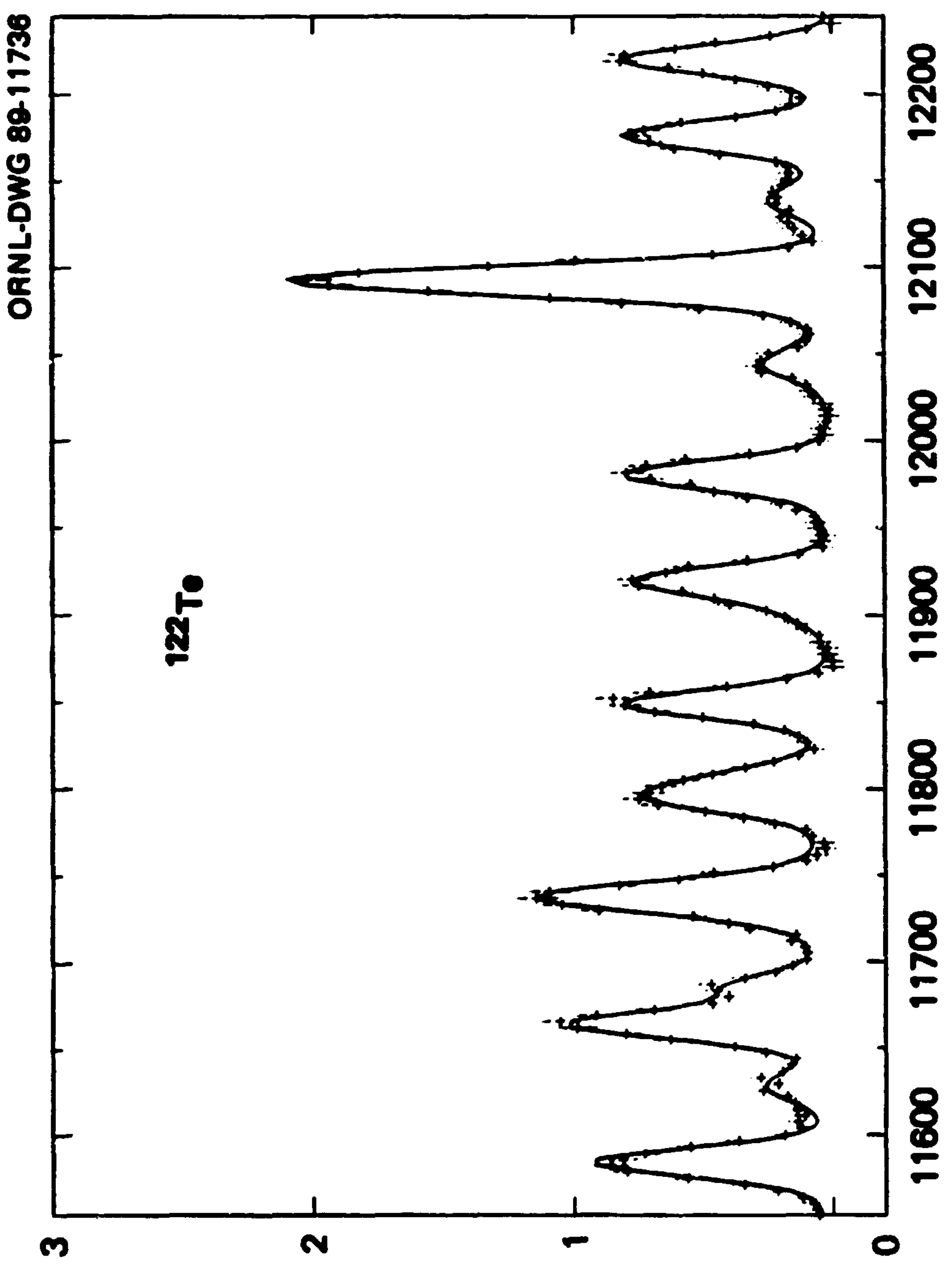

Fig. 2. The ^{122}Te neutron capture data near 12 keV. The symbols represent the data points and their statistical standard deviations. The solid curve corresponds to the fitted parameters given in the tables. The tall peak near 12.1 keV was fitted with spin $J = 3/2$, the rest with spin $J = 1/2$.

For ^{125}Te prior transmission data extended to 7.8 keV and the capture resonance analyses were extended that far also. Twenty-one single peaks below 5 keV were fitted as singlets assuming $l = 0$, $J = 1$. Five of these had been assigned previously (Mughabghab, 1984) and had neutron widths, $2g\Gamma_n$, greater than 100 meV. Only two were broad enough to find a total width from the capture data alone. The average radiation width found was $\Gamma_\gamma = (107.5 \pm 4.1)$ meV with a standard deviation of 18.9 meV corresponding to a chi square distribution with 65 degrees of freedom. One resonance fitted assuming $J = 0$ had a radiation width of 100 meV.

For ^{126}Te four resonances below 6 keV were broad enough to find total widths from the capture data alone. Assuming they had $J = 1/2$ (and were s-wave) their average radiation width was only $\Gamma_\gamma = 53$ meV. As much larger radiation widths had been reported (Mughabghab, 1984), eight more single peaks up to 12.5 keV with reported neutron widths exceeding 500 meV were analyzed. The average radiation width for all twelve was $\Gamma_\gamma = (70 \pm 11)$ meV with a standard deviation of 39 meV, corresponding to a chi square distribution with only 6 degrees of freedom. A resonance at 10.567 keV, assumed $l = 1$, $J = 3/2$ was fitted with a radiation width of 167 meV. Capture peaks were sufficiently isolated to continue the fitting up to 55 keV as shown in Fig. 3.

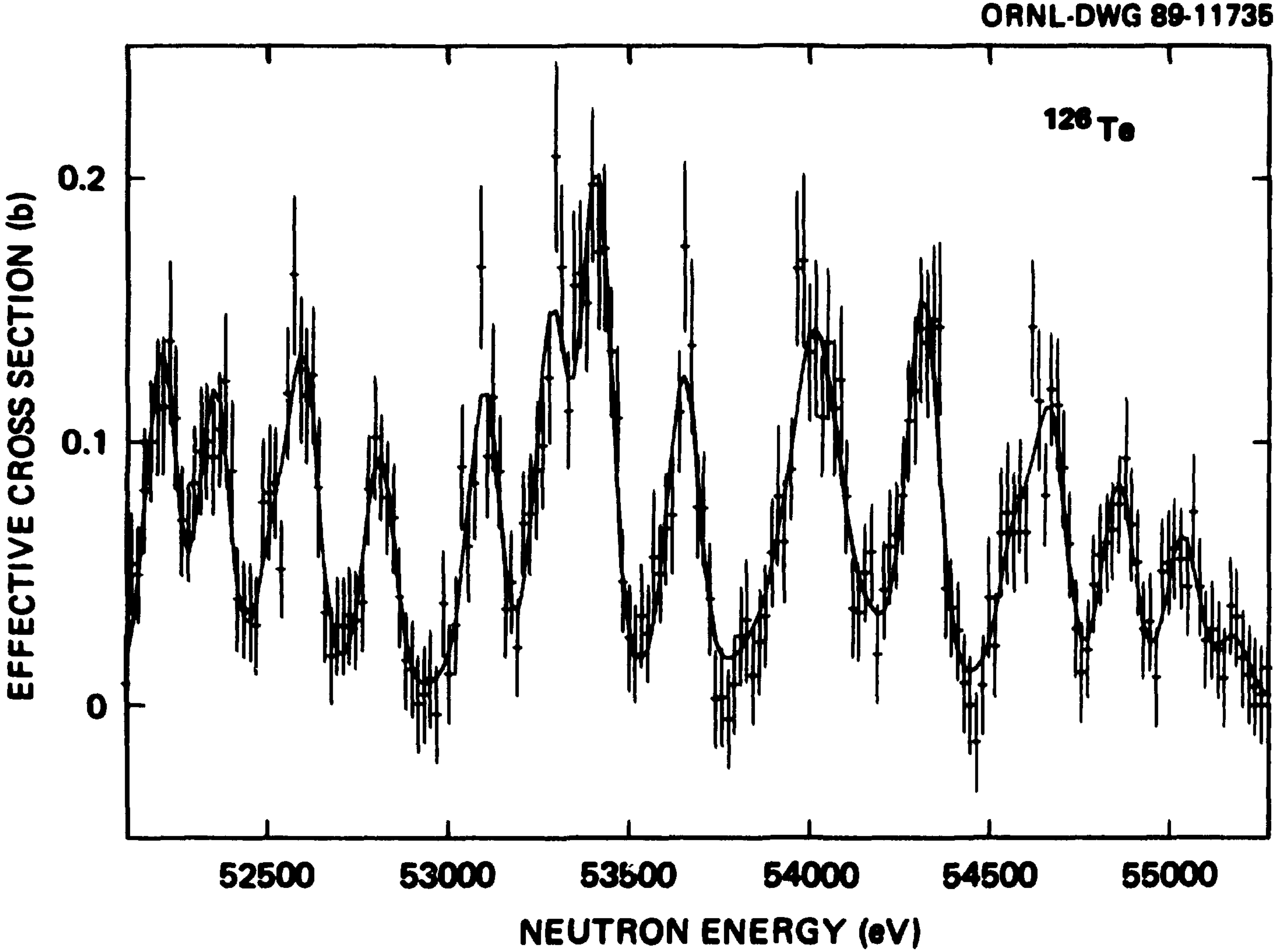

Fig. 3. The ^{126}Te neutron capture data from 52 keV to 55 keV. The symbols represent the data points and their statistical standard deviations. The solid curve corresponds to the fitted parameters given in the tables. While many well-defined peaks could be fitted to the data at higher energies, the attempt to describe the data between them as individual resonances would become increasingly arbitrary.

6. AVERAGE CROSS SECTIONS

The average capture cross sections for the three even mass, spin 0 ground state, tellurium isotopes we measured show sharp decreases with increasing neutron energy just above their thresholds for inelastic neutron scattering to the first spin 2 state. These thresholds are at 569, 607 and 671.5 keV for the tellurium isotopes 122, 124 and 126 respectively. For the two odd mass, spin 1/2 ground state, isotopes such strong inelastic competition was only seen for the second spin 3/2 states with thresholds at 444 and 447 keV and the first spin 5/2 states with slightly higher thresholds. The first spin 3/2 states with thresholds at 159 and 35.5 keV for ^{123}Te and ^{125}Te respectively showed no clear inelastic competition cusps in the capture cross sections.

Histograms of the average cross sections are given in Table 8 and Figs. 4 and 5.

Table 8. Average Neutron Capture Cross Sections

E_n (keV)	^{122}Te (mb)	^{123}Te (mb)	^{124}Te (mb)	^{125}Te (mb)	^{126}Te (mb)
3- 4	879.	2569.	420.	1359.	157.
4- 6	677.	1661.	496.	886.	241.
6- 8	610.	1667.	384.	938.	219.
8- 10	548.	1382.	375.	838.	153.
10- 15	490.	1229.	263.	765.	173.
15- 20	422.	1060.	253.	616.	179.
20- 30	307.	902.	179.	545.	113.
30- 40	259.	774.	136.	423.	79.3
40- 60	213.	659.	117.	324.	68.0
60- 80	181.	553.	91.2	225.	53.2
80-100	155.	484.	83.2	186.	44.6
100-150	137.	430.	72.5	148.	38.5
150-200	133.	347.	71.0	123.	38.4
200-300	132.	271.	72.8	114.	41.1
300-400	132.	232.	72.5	102.	41.6
400-500	142.	214.	78.8	92.3	42.7
500-600	137.	158.	78.3	71.1	43.3

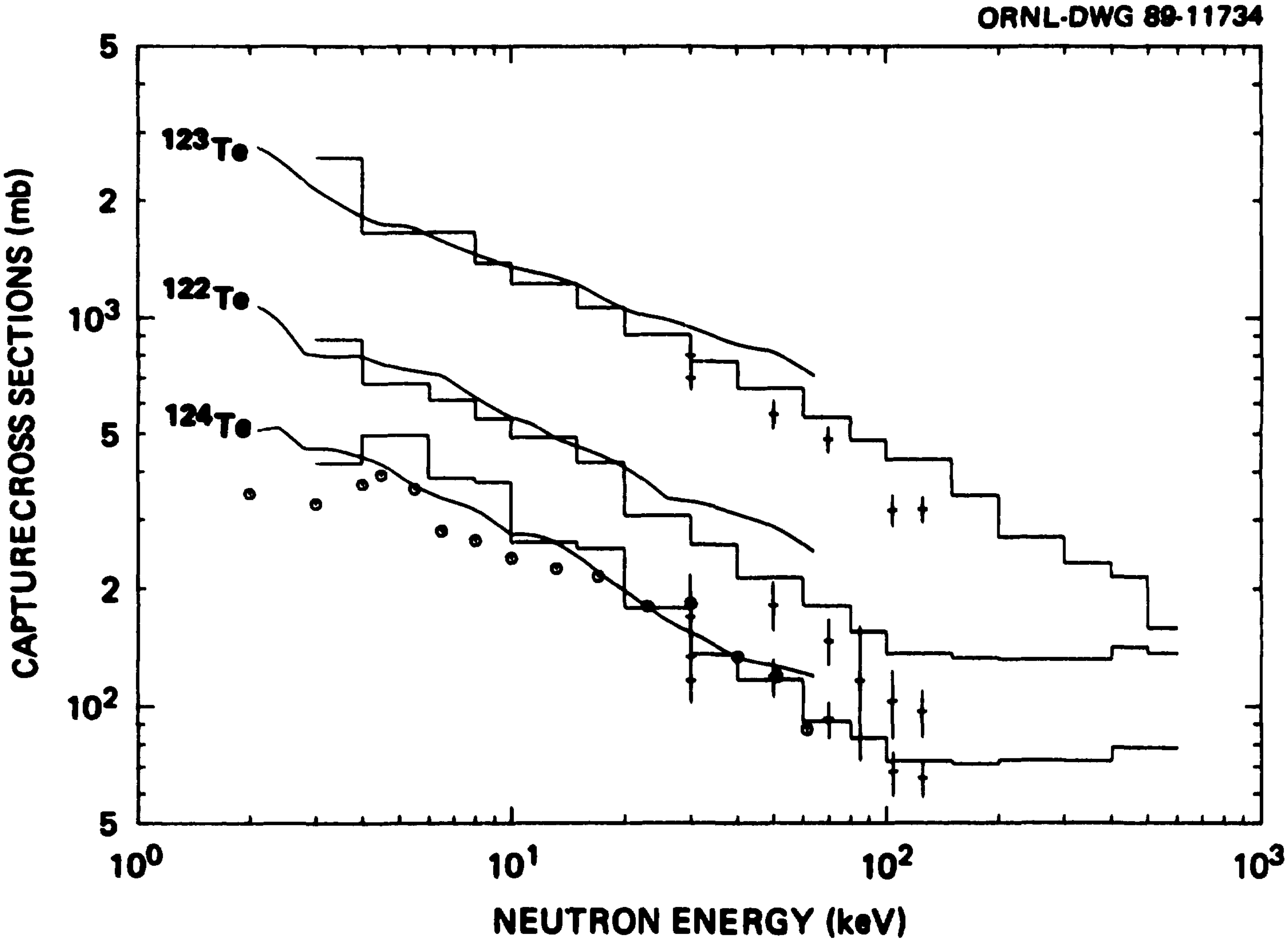

Fig. 4. Average capture for the three *s*-only tellurium isotopes. The solid lines represent the data of Bergman and Romanov (1974), the circles Bergman et al. (1965), and the crosses Macklin and Gibbons (1967a). The solid histograms represent the present data. Numerical values are included in Table 8 and uncertainty estimates in Table 10.

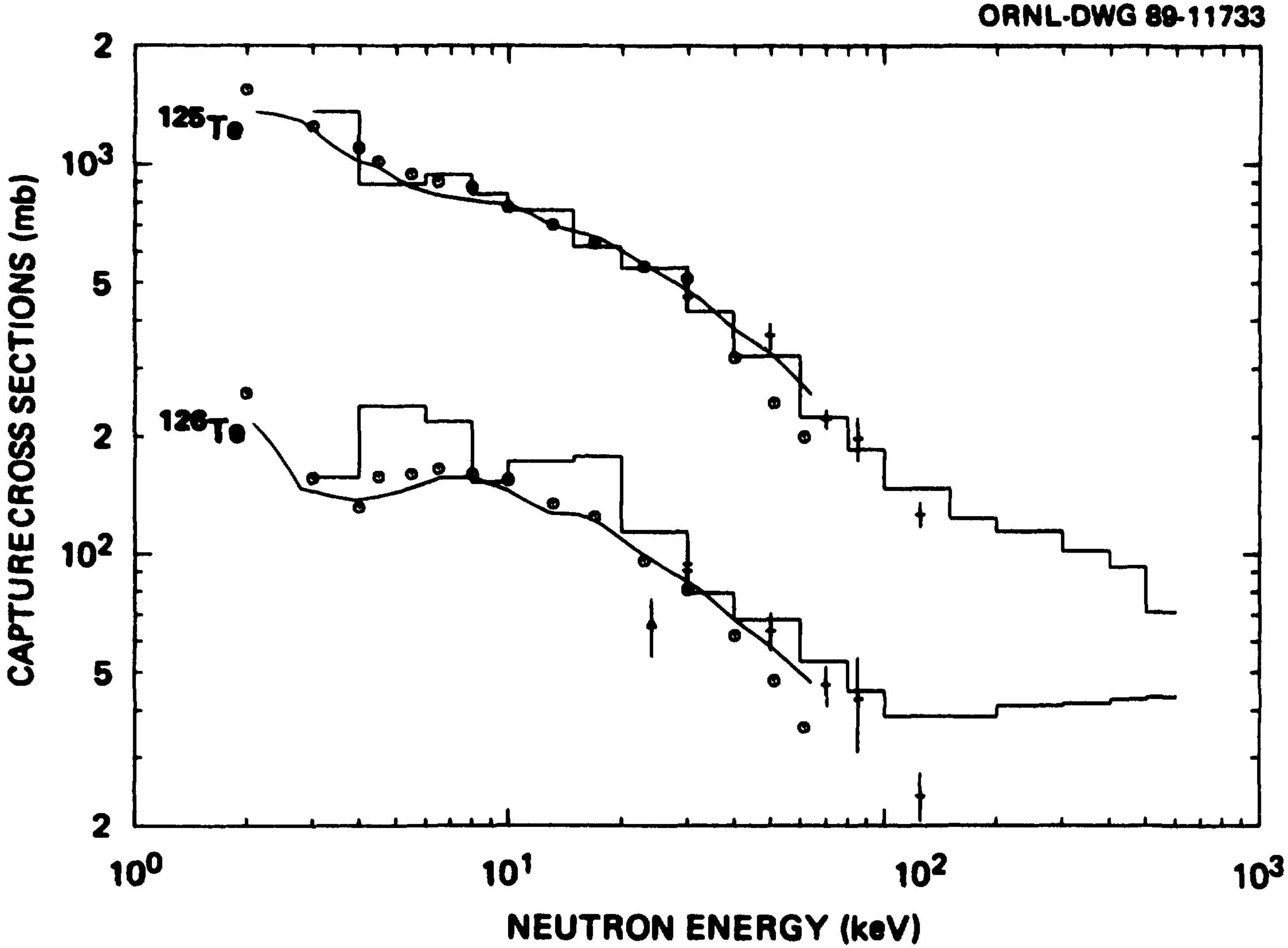

Fig. 5. Average capture of ^{125}Te and ^{126}Te. The solid lines represent the data of Bergman and Romanov (1974), the circles Bergman et al. (1965), the crosses Macklin and Gibbons (1967a), and the triangle Chaubey and Sehgal (1965). The solid histograms represent the present data. Numerical values are included in Table 8 and uncertainty estimates in Table 10.

7. UNCERTAINTIES

Instrumental uncertainties, primarily gain drift of the electronics and phototubes have been tabulated previously (Beer and Macklin, 1982). The gain drifts observed before, between and after our experimental runs using long-lived radioactive sources fell within a 0.34% range with uncertainties on each observation of about 0.06%. The resultant uncertainty in the cross-section results is estimated as ±0.2%.

One of the uncertainties that is particularly difficult to evaluate has to do with the gamma-ray energy weighting function used in processing the capture pulse-height data. Recent work (Perey et. al., 1988) using the Monte Carlo gamma cascade code EGS4 has given weighting functions for our apparatus differing significantly from the one we have used since 1969. The most prominent feature of the new weight functions is the lower weight given to pulse-heights above a few MeV. The capture calculated from measurements of the 115-keV iron-56 resonance, dominated by ~7 MeV gamma rays, with the apparatus used in this experiment was reduced by about 6% by use of the newer weight functions. A likely cause is Compton electrons from high-energy gamma rays interacting in the sample. Such electrons lose about 2 MeV in the scintillator cell wall and a beryllium vacuum window but those above 2 MeV or so give increased detector response for high-energy gamma rays compared with the old calculations. The probability for a 7-MeV gamma ray to give a Compton electron above 2 MeV in one of the tellurium samples should be about 3% compared with about 12% for the 50-g nickel sample for which EGS4 response curves in our apparatus and a weight function have been calculated. The difference in shape of the older weight function and the newer one for the thick Ni sample can be seen in Fig. 6. The larger values of the newer weight function below 1 MeV result from direct inclusion of the 156-keV bias. The older weight function goes to zero at zero pulse height, and the missing data below the bias was treated as a small correction to the total area under the weighted spectrum, typically less than 2%. An estimate of the effect of using this newer weight function on the tellurium isotope data has been derived from the total pulse-height spectrum (i.e., for all neutron energies recorded above 2.6 keV) for each sample. Figure 7 shows the two weighted pulse-height spectra for ^{122}Te as an example. The weighting functions are each normalized separately but arbitrarily. Thus the ratios of the areas for each of the other isotopes to that of the ^{122}Te was calculated and compared with the same ratios using the newer weight function. For the odd isotopes whose spectra extended to 10 MeV the ratio of ratios decreased 2.1% and 1.8% respectively. For the ^{124}Te and ^{126}Te the ratios increased by 1.0% and 3.4% respectively although all the even isotope net spectra were insignificant above 7.6 MeV. The root mean square change of a ratio due to the change of weight function shape from these data was 2.3% and since the 6-g tellurium samples are much smaller than the 50-g nickel sample, it is taken as representative of the uncertainty in weight function.

Table 10. Uncertainty Estimates

Source	Effect (± %)
Average constant and time-dependent backgrounds	1.1
Oxide effects	0.1
Saturated resonance calibration	1.5
Flux monitor efficiency	<3.1[a]
Neutron scattering and absorption by the samples	1.3
Uncertainty in weight function	~2.0
Uncompensated instrumental drifts	0.2
Combined quadrature at 3 keV	3.0
Combined quadrature at 30 keV	3.6
Combined quadrature at 100 keV	3.9
Combined quadrature at 600 keV	4.3

[a]Increased from 0.1 at 3 keV to 3.1 at 600 keV.

ORNL-DWG 89-11732

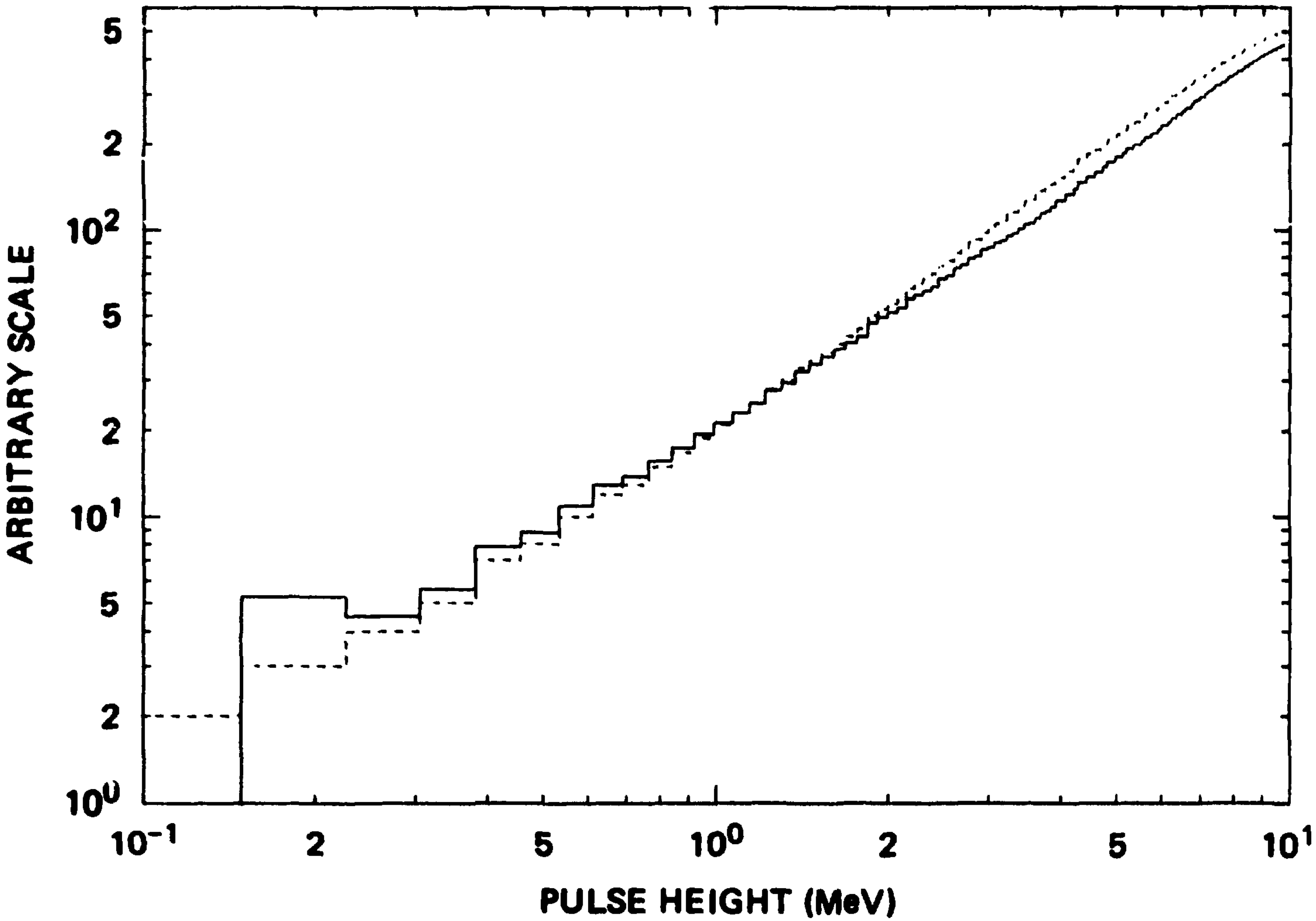

Fig. 6. The Pulse Height Weighting function used in this experiment shown as a dashed histogram, compared with one representative of those calculated for other samples with the gamma cascade code EGS4, shown as the solid line.

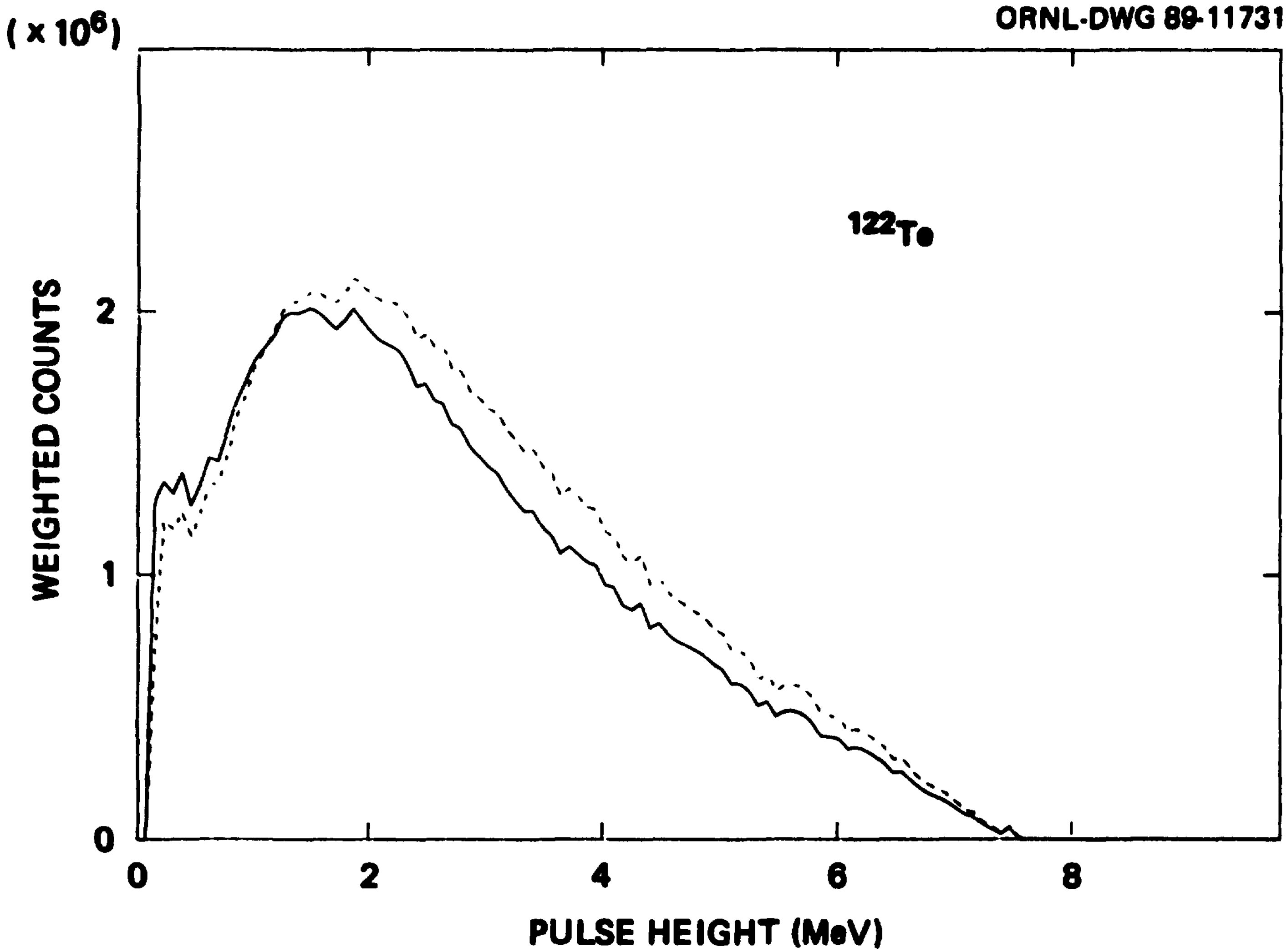

Fig. 7. Pulse height spectra from the ^{122}**Te sample weighted with the two gamma energy weight functions shown in the previous figure.** Gamma-ray energy yields were derived from the areas under the curves and compared with the yields from the four other isotopes to estimate the effect of such a change in weight function (see text).

8. MAXWELLIAN AVERAGE

The stellar velocity-weighted thermal cross section was derived using data from several sources in different energy ranges. Evaluated laboratory thermal capture cross sections from the literature (Mughabghab et al., 1981) were used to evaluate the 1/v capture component and strength functions were used to represent resonance capture below the 2.6-keV neutron energy lower limit of the present measurements. The parameters for the fitted resonances as given in Tables 2 through 7 were used in the next higher energy range and at still higher energies the isotopic yield data as corrected to average cross sections (Table 8) were used. The upper limits for the individual resonance regions were 15.25, 3.75, 27.75, 4.75, and 53.25 keV for the tellurium 122, 123, 124, 125, and 126 isotopes respectively.

The computer code MAXWL (Winters and Macklin, 1987) was used for the calculation at a series of temperatures, $kT = 5$ keV to $kT = 100$ keV, appropriate to stellar nucleosynthesis models. Results are shown in Fig. 8 and Table 9 where the velocity weighted average cross sections are reported in conventional form by dividing the average over the Maxwellian spectrum by the mean thermal velocity at each temperature. At the conventional temperature $kT = 30$ keV the calculations give 280, 819, 154, 423, and 88 mb for ^{122}Te, ^{123}Te, ^{124}Te, ^{125}Te, and ^{126}Te respectively. The uncertainties, ~3.7%, are predominantly systematic ones, estimated at the 68% probability level just as statistical standard deviations are.

Table 9. Maxwellian Average Capture Cross Sections

kT (keV)	^{122}Te (mb)	^{123}Te (mb)	^{124}Te (mb)	^{125}Te (mb)	^{126}Te (mb)
5.0	704 ± 32	1805 ± 83	450 ± 36	1093 ± 53	262. ± 19.
6.0	638 ± 27	1670 ± 71	400 ± 27	1007 ± 45	235. ± 14.
7.0	588 ± 24	1563 ± 63	362 ± 22	939 ± 39	215. ± 12.
8.0	549 ± 22	1476 ± 58	333 ± 18	883 ± 35	199. ± 10.
9.0	517 ± 20	1403 ± 54	310 ± 16	836 ± 33	186. ± 9.
10.0	490 ± 19	1341 ± 50	291 ± 14	795 ± 30	174. ± 8.
12.5	438 ± 16	1216 ± 45	254 ± 11	711 ± 26	152. ± 6.
15.0	399 ± 15	1122 ± 41	228 ± 9	645 ± 24	136. ± 5.
17.5	369 ± 13	1048 ± 38	209 ± 8	592 ± 22	123. ± 5.
20.0	345 ± 13	987 ± 36	193 ± 7	547 ± 20	113. ± 4.
25.0	307 ± 11	892 ± 32	170 ± 6	476 ± 17	98.6 ± 3.7
30.0	280 ± 10	819 ± 30	154 ± 6	423 ± 15	88.3 ± 3.2
35.0	260 ± 9	762 ± 27	142 ± 5	381 ± 14	80.7 ± 2.9
40.0	243 ± 9	714 ± 26	132 ± 5	348 ± 13	74.9 ± 2.7
45.0	230 ± 8	674 ± 24	125 ± 5	321 ± 12	70.3 ± 2.6
50.0	219 ± 8	639 ± 23	119 ± 4	298 ± 11	66.6 ± 2.4
60.0	203 ± 7	582 ± 21	110 ± 4	263 ± 9	61.2 ± 2.2
70.0	191 ± 7	536 ± 19	103 ± 4	237 ± 9	57.4 ± 2.1
85.0	179 ± 6	482 ± 17	97 ± 4	208 ± 8	53.7 ± 1.9
100.0	170 ± 6	440 ± 16	92 ± 4	187 ± 7	51.3 ± 1.9

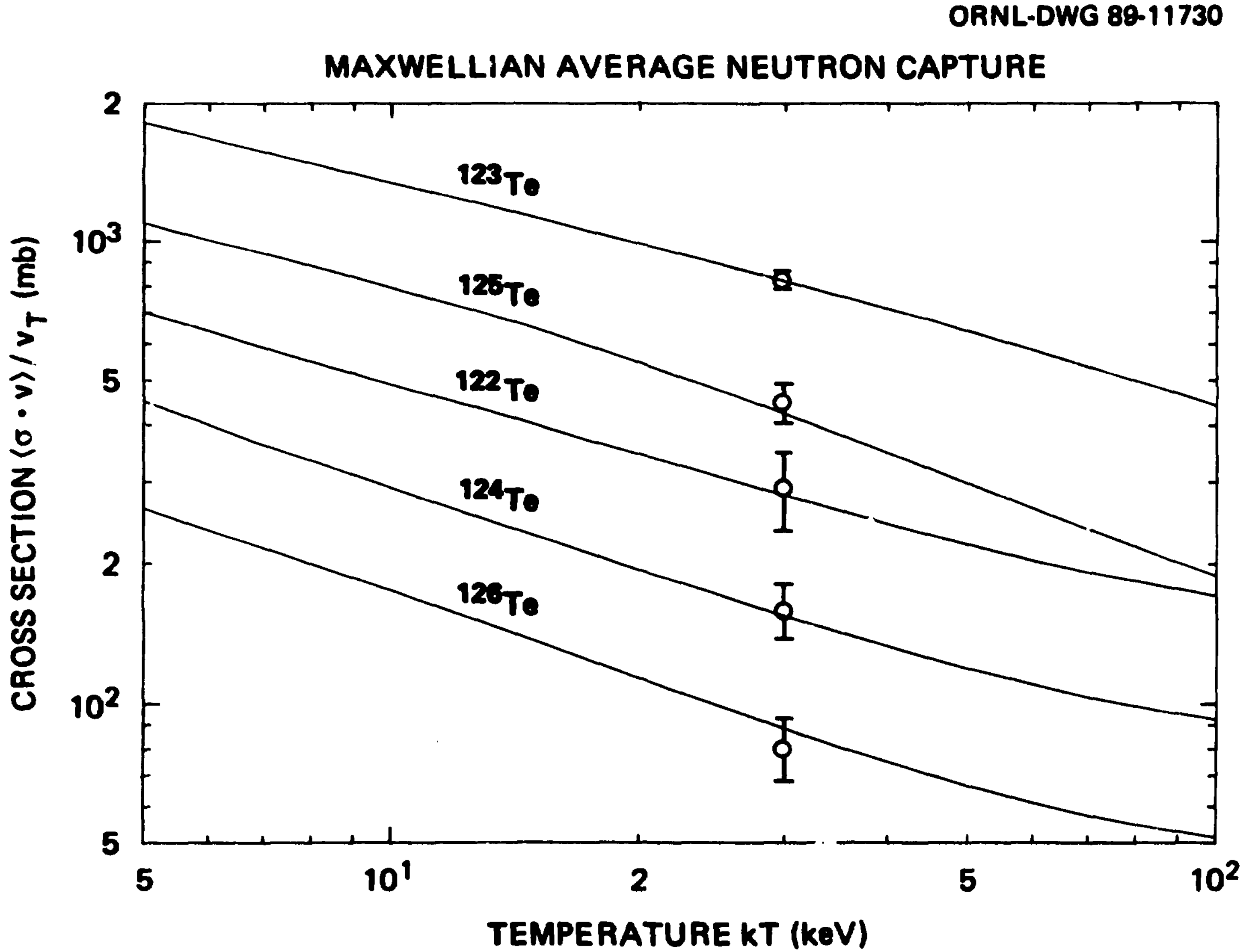

Fig. 8. Maxwellian averaged cross sections vs temperature. The symbols represent the evaluations of Bao and Käeppeler (1987). Numberical values for the present results and their uncertainties are given in Table 9.

9. DISCUSSION

Thirty-three of the broader resonances where both radiation and neutron widths could be determined from our capture data alone, allow direct comparison with parameters from transmission studies (Tellier and Newstead, 1971) listed in a recent evaluation (Mughabghab, 1984). Almost half of these are for ^{122}Te where the reported neutron widths range from 0.42 to 1.16 times those found from fitting the capture data. Seven of those cases, however, agree within the reported uncertainty. For ^{123}Te the reported resonances do not extend above 2 keV so there is no overlap with the capture data which start at 2.6 keV. For ^{124}Te the range is better, 0.84 to 1.10, for eleven resonances; four of them within the reported uncertainties. For ^{125}Te there are only two cases. The reported neutron widths are 0.75 and 0.67 times those found in the present study, but for the first of these an inconsistent total width is also reported, 1.41 times that found from fitting the capture data. For ^{126}Te there are just four comparison resonances with reported neutron widths ranging from 0.50 to 0.98 times ours. Only one is within the reported uncertainty.

Seeger et al. (1965) first showed that the observed heavy element abundances attributable to the stellar *s*-process could be well fitted by an exponential distribution of neutron exposures. Much more detailed stellar models have been developed since, but the near constancy of the product of cross section and abundance as a function of atomic mass near mass 123 is still predicted. A more recent computer code (Beer et al., 1989) shows ratios of 0.996 and 0.976 for mass 123 and mass 124 respectively, when normalized to 1.00 at mass 122.

Solar system abundances have been reevaluated recently (Anders and Grevesse, 1989). For the tellurium isotopes 122-126 respectively, they give 0.124, 0.0428, 0.229, 0.342 and 0.909 per million atoms of silicon. The products of abundance and $kT = 30$ keV Maxwellian average capture for ^{122}Te, ^{123}Te and ^{124}Te respectively, normalized to that for ^{122}Te, become 1.00, 1.009 ± 0.038, and 1.014 ± 0.038. If we take the results of the change in weight function discussed under uncertainties as a correction rather than an uncertainty, these ratios change to 1.00, 0.988 ± 0.032, and 1.024 ± 0.032. Comparable changes in these ratios are seen with changes in assumed stellar temperatures. For example, interpolating linearly in Table 9 for a temperature $kT = 23$ keV, that chosen for the *s*-process calculation by Beer et al. (1989), gives ratios 1.00, 0.996 ± 0.038, and 1.028 ± 0.038.

10. CONCLUSIONS

The $kT = 30$ keV Maxwellian average cross sections found in the present work are in close agreement with the latest compilation (Bao and Käppeler, 1987) which is based primarily on the earlier experimental works (Bergman and Romanov, 1974) and (Macklin and Gibbons, 1967a,b). The uncertainties associated with air oxidation of elemental tellurium samples have been elucidated and the experimental cross-section uncertainties significantly reduced. In combination with the latest abundance evaluation (Anders and Grevesse, 1989), the results for ^{122}Te, ^{123}Te and ^{124}Te agree with the s-process prediction for s-only isotopes of adjacent mass number. Calculations of s-process nucleosynthesis (Beer et al., 1989) correspond to a tellurium elemental abundance about 5% or two standard deviations of the mean below the evaluation. A similar elemental underprediction of (23± 12)% for tin has been noted (Anders and Grevesse, 1989).

REFERENCES

1. Anders, E. and N. Grevesse, *Geochim. Cosmochim. Acta*, **53**, 197 (1989).
2. Bao, Z. Y. and F. Käppeler, *Atomic Data and Nuclear Data Tables*, **36**, 411 (1987).
3. Beer, H. and R. L. Macklin, *Phys. Rev. C*, **26**, 1404 (1982).
4. Beer, H. and R. L. Macklin, "Measurement of the ^{85,87}Rb Capture Cross Section for *s*-Process Studies," *Astrophys. J.* (in press) April 15, 1989.
5. Beer, H., G. Walter and F. Käppeler, *Astron. Astrophys.*, **211**, 245 (1989).
6. Bergman, A. A. and S. A. Romanov, *Yad. Fiz.* **20**,252 (1974) and engl. *Sov. J. Nucl. Phys.*, **20**, 133 (1975).
7. Bergman, A. A., S. P. Kapchigaschev, Yu.P. Popov, and S. A. Romanov, *Proc. Int'l Conf. on the Study of Nuclear Structure with Neutrons*, Antwerp, Belium, July 1965, p. 570, North-Holland, Amsterdam; data from McLane, Dunford and Rose (1988).
8. Browne, J. C. and B. L. Berman, *Phys. Rev. C*, **8**,2405 (1973).
9. Burbidge, E. M., G. R. Burbidge, W. A. Fowler and F. Hoyle *Rev. Mod. Phys.* **29**, 547 (1957).
10. Chaubey, A. K. and M. L. Sehgal, *Nucl. Phys.* **66**, 267 (1965).
11. Käppeler, F., H. Beer, K. Wisshak, D. D. Clayton, R. L. Macklin and R. A. Ward, *Ap. J.*, **257**, 821 (1982).
12. Macklin, R. L., *Nucl. Sci. Eng.* **59**, 12 (1976a).
13. Macklin, R. L., *Nucl. Sci. Eng.* **59**, 231 (1976b).
14. Macklin, R. L., *Nucl. Sci. Eng.* **86**, 362 (1984).
15. Macklin, R. L., D. M. Drake, and E. D. Arthur, *Nucl. Sci. Eng.* **84**, 98 (1983).
16. Macklin, R. L. and J. H. Gibbons, *Phys. Rev.* **159**, 1007 (1967a).
17. Macklin, R. L. and J. H. Gibbons, *Ap. J.* **194**, 577 (1967b).
18. Macklin, R. L., J. Halperin, and R. R. Winters, *Nucl. Instrum. Methods* **164** 213 (1979).
19. Macklin, R. L., R. W. Ingle, and J. Halperin, *Nucl. Sci. Eng.* **71**, 205 (1979).
20. McLane, V., C. L. Dunford, and P. F. Rose, *1988 Neutron Cross Sections*, Vol. 2, Academic Press, New York.
21. Mughabghab, S. F. *1984 Neutron Cross Sections*, Vol.1, Part B, Academic Press, New York.
22. Perey, F. G., J. O. Johnson, T. A. Gabriel, R. L. Macklin, R. R. Winters, J. H. Todd, and N. W. Hill, *1988 Nuclear Data for Science and Technology, Proceedings of the International Conference at Mito, Japan, May 30-June 3, 1988*, ed. S. Igarasi, page 379; and Perey, F. G., private communication, 1988.
23. Seeger, P. A., W. A. Fowler, and D. D. Clayton *Ap. J. Suppl.* **11**, 121 (1965).

24. Tellier, H. and C. M. Newstead, *1971 Neutron Cross Sections and Technology, Proceedings of the Third Conference* at Knoxville, Tennessee, March 15-17, 1971, ed. R. L. Macklin, page 680.

25. Winters, R. R. and R. L. Macklin, *Ap. J.* **313**, 808 (1987).

26. Yamamuro, N., Hayase, T., Doi, T., Fujita, Y., Kobayashi, K., and Block, R. C., *Nucl. Instr. Meth.* **133**, 531 (1976).

INTERNAL DISTRIBUTION

1. B. R. Appleton
2. G. de Saussure
3. J. K. Dickens
4. C. Y. Fu
5. R. Gwin
6. J. A. Harvey
7–11. R. L. Macklin
12. F. C. Maienschein
13. R. W. Peelle
14. F. G. Perey
15–19. R. B. Perez
20. S. A. Raby
21. R. R. Spencer
22. L. W. Weston
23–27. R. R. Winters
28. J. J. Dorning (consultant)
29. R. M. Haralick (consultant)
30–31. Laboratory Records Department
32. Laboratory Records, ORNL-RC
33. Document Reference Section
34. Central Research Library
35. ORNL Patent Section

EXTERNAL DISTRIBUTION

36. Office of Assistant Manager for Energy Research and Development, Oak Ridge Operations, U.S. Department of Energy, Oak Ridge, TN 37831
37. E. D. Arthur, Los Alamos National Laboratory, Los Alamos, NM 87545
38. H. Beer, Kernforschungszentrum Karlsruhe, Institut fur Kernphysik III, Postfach 3640, D-7500 Karlsruhe 1, Federal Republic of Germany
39. R. C. Block, Department of Nuclear Engineering, Rensselaer Polytechnic Institute, Troy, NY 12181
40. D. D. Clayton, Rice University, Department of Space Physics and Astronomy, P. O. Box 1892, Houston, TX 77251
41. F. Corvi, Bureau Central de Mesures Nucleaires, Steenweg naar Retie, B-2440 Geel, Belgium
42. B. Fogelberg, The Studsvik Science Research Laboratory, S-611, 82 Nyköping, Sweden
43. W. A. Fowler, California Institute of Technology, W. K. Kellogg Radiation Laboratory, 1201 California Blvd., Pasadena, CA 91125
44. F. H. Fröehner, Institut fur Neutronenphysik und Reaktortechnik, Kernforschungszentrum Karlsruhe, Postfach 3640, 7500 Karlsruhe, Federal Republic of Germany
45. F. Käppeler, Institut fur Neutronenphysik und Reaktortechnik, Kernforschungszentrum Karlsruhe, Postfach 3640, 7500 Karlsruhe, Federal Republic of Germany
46. Y. Kikuchi, Nuclear Data, Division of Physics, Japan Atomic Energy Research Institute (JAERI), Tokai-mura, Naka-gun, Ibaraki-ken 319-11, Japan
47. C. Lagrange, Service de Physique Neutronique et Nucleaire, Centre d'Etudes de Bruyeres-le-Chatel, B.P. No. 561, 92542 Montrouge, Cedex, France
48. V. McLane, National Nuclear Data Center, Brookhaven National Laboratory, Upton, NY 11973
49. M. Mizumoto, Japan Atomic Energy Research Institute, Tokai-mura, Naka-gun, Ibaraki-ken, Japan

50. R. E. Schenter, Hanford Engineering Development Laboratory, Westinghouse Hanford Company, P. O. Box 1970, Richland, WA 99352
51. A. B. Smith, Argonne National Laboratory, 9700 S. Cass Avenue, Argonne, IL 60439
52. M. G. Sowerby, Nuclear Physics Division, Building 418, Atomic Energy Research Establishment, Harwell, Didcot, Oxon OX11 ORA, United Kingdom
53. S. L. Whetstone, Division of Nuclear Sciences, Office of Basic Energy Sciences, U.S. Department of Energy, Room G-355, Washington, DC 20545
54. H. Weigmann, Bureau Central de Mesures Nucleaires, Steenweg naar Retie, B-2440, Geel, Belgium
55–64. Office of Scientific and Technical Information, P. O. Box 62, Oak Ridge, TN 37830